DOI:
10.1126/scisignal.aaw2418

Document Version
Peer reviewed version

One-sentence summary: Nanoscale reorganization of TNFR1 within the plasma membrane promotes the activation of distinct signaling pathways.

Editor's summary:

Organizing TNFR1 signaling

The inflammatory cytokine tumor necrosis factor α (TNF-α) stimulates both cell death and survival by activating its ubiquitously expressed membrane receptor, TNFR1. Morton *et al*. used various microscopy techniques to investigate TNFR1 membrane organization. In resting cells, TNFR1 was found within clusters that required its cytoplasmic tail. After TNF-α binding, TNFR1 clusters were denser and moved within the membrane more rapidly, which correlated with the activation of specific downstream pathways and physical association with the kinase MEKK1. Experiments with engineered ligands that could only bind a specific number of TNFR1 molecules suggested that engagement of two receptors was sufficient for signaling, but that trimeric interactions were necessary for extracellular conformational changes in TNFR1. These findings suggest how membrane organization alters TNFR1 signaling, insights that may direct the development of TNF-targeted therapeutics with increased potency.

TNFR1 membrane reorganization promotes distinct modes of TNFα signaling

Penny E. Morton[1], Camille Perrin[1], James Levitt[1], Daniel R. Matthews[2], Richard J. Marsh[1], Rosemary Pike[1,5], David McMillan[3], Alison Maloney[3], Simon Poland[1,4], Simon Ameer-Beg[1,4], Maddy Parsons[1,6]

[1] Randall Centre for Cell and Molecular Biophysics, King's College London, New Hunts House, Guys Campus, London SE1 1UL
[2] Nikon Imaging Centre, King's College London, Hodgkin Building, Guys Campus, London, SE1 1UL
[3] UCB Celltech, 208 Bath Road, Slough, SL1 3WE
[4] School of Cancer and Pharmaceutical Sciences, King's College London, New Hunts House, Guys Campus, London SE1 1UL
[5] Current address: Cancer Research UK Therapeutic Discovery Laboratories, London Bioscience Innovation Centre, 2 Royal College Street, London NW1 0NH
[*] Corresponding author. Email: maddy.parsons@kcl.ac.uk

Abstract

Signaling by the ubiquitously expressed tumor necrosis factor receptor 1 (TNFR1) after ligand binding plays an essential role in determining whether cells exhibit survival or death. TNFR1 forms distinct signaling complexes that initiate gene expression programs downstream of the transcriptional regulators NF-κB and AP-1 and promote different functional outcomes, such as inflammation, apoptosis, and necroptosis. Here, we investigated the ways in which TNFR1 was organized at the plasma membrane at the

nanoscale level to elicit different signaling outcomes. We confirmed that TNFR1 forms pre-assembled clusters at the plasma membrane of adherent cells in the absence of ligand. After trimeric TNF-α binding, TNFR1 clusters underwent a conformational change, which promoted lateral mobility, their association with the kinase MEKK1, and activation of the JNK/p38/NF-κB pathway. These phenotypes required a minimum of two TNFR1–TNF-α contact sites; fewer binding sites resulted in activation of NF-κB but not JNK and p38. These data suggest that distinct modes of TNFR1 signaling depend on nanoscale changes in receptor organization.

Introduction

Tumor necrosis factor α (TNFα) is a master pro-inflammatory cytokine and dysregulated TNF signaling is implicated in the pathology of a broad range of inflammatory diseases (1). TNFα binds to TNF-receptor 1 (TNFR1), which is a member of the TNFR superfamily of which there are 29 known members. Most members of the TNFR superfamily contain cysteine-rich domains (CRDs) in the extracellular domain (2). TNFRs are thought to exist as preassembled oligomers on the cell surface, mediated by the pre-ligand assembly domain (PLAD) that resides within the N-terminal CRD1 that is not directly involved in ligand-binding (3). Soluble PLAD can prevent TNFR signaling and inhibit inflammatory arthritis, suggesting that PLAD-mediated receptor assembly is required for TNFR signaling (4). Mutations within CRD1 and CRD2 that are thought to render TNFR1 constitutively active are also associated with the inflammatory disease TNF Receptor associated periodic syndrome (TRAPS) (5, 6). However, crystal structures of TNF-TNFR superfamily complexes, including TNFR1 itself, suggest individual PLADs are disassociated (7). Further X-ray structure analysis of the TNF-TNFR2 complex in solution demonstrates that in the absence of ligand, receptors assemble as parallel or anti-parallel dimers (8, 9). The potential relevance of these solution structures to receptor signaling within intact cells remains unclear as do the potential molecular changes in TNFR1 that occur in response to different context-dependent stimuli.

TNFR1 also contains a Death Domain (DD) within cytoplasmic tail that recruits adaptor molecules leading to the assembly of signaling complexes (I and IIa/b/c) that promote distinct functional outcomes (10). After TNF binding, complex I is assembled at TNFR cytoplasmic domains at the plasma membrane and comprises TNFR1-associated death domain protein (TRADD), receptor-interacting serine/threonine-protein kinase 1 (RIPK1), TNFR-associated factor 2 (TRAF2), cellular inhibitor of apoptosis protein 1 (cIAP1) or cIAP2, and linear ubiquitin chain assembly complex (LUBAC). The current evidence suggests that TRAF2 and cIAP1/cIAP2 ubiquitinylate complex I components and the LUBAC complex adds further linear ubiquitin chains to stabilize and amplify signaling (11, 12). Recruitment and activation of the transforming growth factor (TGF)-β-activated kinase 1 (TAK1) complex and the inhibitor of κB (IκB) kinase (IKK) complex then activates unique downstream effectors. TAK1 is involved in activating mitogen-activated kinase (MAPK) signaling cascades that lead to activation of JUN N-terminal kinase (JNK), p38 and AP1 transcription factor, whereas IKKβ activates the canonical nuclear factor κB (NFκB) pathway (11, 13). Induction of signaling complex I leads to the expression of AP1 and/or NFκB target genes that are important in inflammation, cell proliferation and survival. However, the way in which TNFR1 complexes are fine-tuned to initiate differential signaling upon assembly of complex I remain unknown.

TNFR1 is proposed to be a pre-formed dimer at minimum, but assumed to form higher ordered clusters on ligand binding in order to initiate signaling (3). Furthermore, cholesterol-rich lipid raft domains and palmitoylation modifications may be required for TNFR1 signaling after ligand binding by promoting coalesce of pre-assembled TNFR1 clusters to form functional signaling platforms (14, 15). However, lipid rafts are not required for TNFR1-induced NFκB signaling responses to ligand (16, 17). Given the essential role of TNFR1 in mediating cell behavior under homeostatic and inflammatory conditions, understanding the way in which TNFR1 assembles and signals at the plasma membrane is of central importance to defining the role of this receptor in disease settings. Here we employed a combination of biochemical and advanced microscopy approaches in adherent cells to define the role of TNF-TNFR1 interactions in promoting receptor clustering and specific signaling events. Our findings revealed that TNFR1 formed pre-assembled clusters at the plasma membrane of adherent cells in the absence of ligand and this was independent of cholesterol and extracellular TNFR1 interactions, but partly dependent on the presence of the cytoplasmic domain. Trimeric TNFα binding induced conformational change within the ectodomain of TNFR1 leading to lateral TNFR1 cluster mobility, TNFR1-MEKK1 association and initiation of JNK/p38/NFκB activation. These phenotypes all required a minimum of 2 TNFR1-TNFα contact sites, as fewer binding sites initiated NFκB activation, but not JNK/p38. This data demonstrates that distinct modes of TNFR1 signaling depend on nanoscale changes in receptor organization and conformation.

Results

TNFR1 forms ligand-independent higher-ordered clusters at the plasma membrane

In order to determine the organization of TNFR1 at the plasma membrane, we first analyzed the localization of TNFR1 in adherent cells using both widefield and total internal reflection fluorescence (TIRF) microscopy. Images demonstrated that in starved HeLa cells, TNFR1 was clustered within the cytoplasm around the peri-nuclear region with small, irregularly positioned clusters of TNFR1 at the plasma membrane (Fig S1A). This pre-clustered localization of TNFR1 at the plasma membrane was also observed in a range of other adherent cell types (Fig S1B). In order to allow us to study the behavior of these TNFR1 clusters in live cells, we generated TNFR1 knockdown HeLa cells (Fig S1C) and re-expressed full-length, wild-type (WT) TNFR1-GFP in these cells. Expressed TNFR1-GFP bound to TNFα (Fig S1D), showed very similar co-localization at the plasma membrane as endogenous TNFR1 (Fig 1A, and fig S1E) and restored TNF-dependent signaling to NFκB in TNFR1 depleted cells (Fig S1F, G). We next tested whether the size or number of TNFR1 clusters at the plasma membrane changed in response to TNFα treatment. Analysis of TIRF images of TNFR1-GFP or those counter-stained for TNFR1 demonstrated no change in the distribution of cluster sizes in cells after treatment (Fig 1A) and a very similar result was obtained from images of endogenous TNFR1 in parental HeLa cells (Fig S1H). Together, these data indicated TNFR1 was constitutively clustered at the plasma membrane in adherent cells and TNFα binding did not alter the size or distribution of these clusters, as measured by diffraction-limited imaging.

In order to determine whether the extracellular regions of TNFR1 contributed to the pre-formed clusters at the plasma membrane, we expressed three different mutant forms of TNFR1-GFP in TNFR1 knockdown cells: R92Q (within CRD2) or C52F (within CRD1), previously characterized in patients with TRAPS (18), as well as a quadruple point mutation within CRD1 predicted to destabilize putative pre-formed associations through CRD1 (Q17A/K19A/H34A/D49A). When we compared the distribution of each receptor mutant to WT TNFR1 by TIRF microscopy, we found no substantial change in plasma membrane clustering with any of the mutants compared to WT TNFR1 (Fig 1B). We also expressed TNFR1-GFP lacking the cytoplasmic domain (ΔCD) to determine whether pre-formed clusters were instead due to formation of associated complexes at the cytoplasmic face of the receptor. In the absence of the CD, TNFR1 diffusely localized at the plasma membrane and was still able to assemble into discrete clusters (Fig 1B) . Moreover, co-expression of WT and ΔCD or AAAA mutants of TNFR1 revealed no colocalization between the WT and mutant receptors at the membrane (Fig 1C), suggesting that specific conformations of TNFR1 may preferentially co-associate into membrane clusters. This data suggests that formation of TNFR1 clusters in the absence of ligand may not depend on previously reported regions within the extracellular domains (19), but that the presence of the cytoplasmic tail can potentially stabilize these higher-ordered complexes at the plasma membrane.

Our data showed no change in TNFR1 cluster size or number in cells following ligand binding using diffraction limited microscopy methods. In order to determine whether interactions between individual receptors were altered at the nanoscale, we analyzed fluorescence resonance energy transfer (FRET) between co-expressed GFP and RFP labelled WT TNFR1 homodimers using fluorescence lifetime imaging microscopy (FLIM). In agreement with our TIRF images, FRET efficiency analysis demonstrated a high degree of pre-formed clustering in starved cells, but a significant increase in direct TNFR1 homo-interactions following TNFα binding (Fig 1D) that corresponded with a shift to lower lifetimes across the receptor population (Fig S2A). In cells expressing ΔCD TNFR1, we observed similar interactions between receptors, which were not increased by ligand binding (Fig 1D). Notably, there was no detectable FRET between WT TNFR1 and ΔCD TNFR1 with or without TNFα (Fig S2C), which confirmed that TNFR1 WT and mutant forms preferentially homo-oligomerize.

Nanoscale organization of TNFR1 pre-assembled clusters changes following ligand binding

Our FRET data demonstrated that TNFR1 homo-oligomerization increases following TNFα treatment, but without changes in the overall cluster size or number by diffraction-limited microscopy. In order to determine whether TNFR1 may undergo exchange between discrete clusters during activation to drive this increased homo-oligomerization, we performed fluorescence recovery after photobleaching (FRAP) analysis of cells co-expressing TNFR1-GFP and TNFR1-mRFP. TNFR1-GFP was bleached and recovery analyzed following TNFα stimulation whilst simultaneously following the unbleached TNFR1-RFP to accurately track the cluster. Recovery curves demonstrated no new TNFR1-GFP was recruited to clusters following activation (Fig 2A). These data suggest that there is no detectable exchange of receptors between clusters following ligand binding. To further define the potential changes to TNFR1 organization within clusters, we used stochastic

optical reconstruction microscopy (STORM) to quantify positioning of individual TNFR1 molecules at the plasma membrane before and after ligand binding. From the detected individual localizations, we determined that TNFα stimulation of cells did not change the number of localizations per area (Fig 2B, C), or the percentage of localizations identified that were positioned within categorized high (Fig 2D) or low (Fig 2E) density clusters. However, a significant increase in the proportion of TNFR1 clusters containing high density, closely packed molecules was observed in TNFα-activated compared to starved cells (Fig 2F). These data are in agreement with our FLIM data showing increased receptor proximity under these conditions (Fig 1D) and suggest that TNFR1 forms pre-assembled clusters, which increased in local density at the nanoscale following TNFα binding,

TNFR1 clusters undergo dynamic re-positioning on the plasma membrane following ligand binding

Our data indicated that ligand binding altered the organization of TNFR1 clusters, similar to other receptor families after activation (20, 21). We next analyzed whether this was also associated with movement of the clusters using time-lapse imaging by TIRF microscopy. We found that TNFR1 clusters moved slowly within the plasma membrane in unstimulated cells, but TNFα treatment significantly increased cluster movement speed (Fig 3A). Further analysis of particle tracks demonstrated no correlation between cluster size and movement speed (Fig 3B). Because TNFR1 is internalized in certain cell types to promote apoptosis (22-24), we next addressed the extent of endocytosis in HeLa cells after TNF binding. We found that ligand binding did not promote TNFR1 internalization for up to 2 hours post-treatment using biotin pulse chase experiments (Fig 3C). In order to further confirm that endocytosis was not required for TNFR1 activation, we treated cells with the Dynamin2 inhibitor Dynasore and analyzed activation of NFκB and JNK. Inhibiting Dynamin function had no impact on activation of either pathway (Fig 3D) or localization of TNFR1 (Fig S3C). These data demonstrated that endocytosis did not play a role in TNFR1 activation under these conditions tested in adherent cells and is therefore unlikely to account for the TNFR1 cluster movement we observed. We also addressed the possibility that TNFR1 ectodomain cleavage may contribute to cluster movement, as TNFR1 has previously been show to undergo cleavage within the ectodomain by the enzyme TACE (25, 26). However, western blot analysis for TNFR1 cytoplasmic domain following ligand stimulation did not reveal lower molecular weight bands and no change in TNFR1 banding pattern was seen after pre-treatment with the TACE inhibitor TAPI-0 (Fig S3A). These data indicated that TNFR1 does not undergo cleavage events that might explain the cluster movement we that observed under these conditions within the time frames analyzed.

The organization of the plasma membrane into microdomains may alter TNFR1 partitioning and subsequently promote signal transduction from the plasma membrane in some cell types (16, 27). In order to determine whether cholesterol-rich microdomains partition TNFR1 in adherent cells, we firstly stained cells with Cholera toxin to determine whether TNFR1 localized to GM1-containing lipid rafts. We found no overlap between TNFR1-GFP and Ctx-Alexa555 in starved or TNFα treated cells and TNFR1 clusters were still present in cells treated with the cholesterol-depleting agent methyl-β-cyclodextran (MβCD) (Fig 3E). TNFR1 clusters also did not colocalize with clathrin (Fig S3B) and alter localization was not

altered by treatment with Cytochalasin D, which disrupts the actin cytoskeleton, or Nocodazole, which disrupts microtubule polymerization (Fig S3C). TNFα treatment did not stimulate cleaved caspase (Fig S3D), which indicates that TNFα-induced cluster movement does not trigger apoptosis in these cells, and is in agreement with the notion that internalized receptors predominantly initiate cell death. These data combined demonstrated that pre-formed TNFR1 clusters did not reside in cholesterol-rich microdomains in these adherent cells and did not require the cytoskeleton for pre-assembly.

To determine whether the cytoplasmic regions of TNFR1 clusters contributed to the cluster movement, we performed TIRF time-lapse analysis of cells expressing ΔCD-TNFR1. We observed that in comparison to WT TNFR1, plasma membrane localization of the mutant receptor lacking the cytoplasmic region was increased. Despite this, ΔCD TNFR1 assembled clusters that exhibited higher basal movement and did not alter speed in response to ligand binding compared to WT TNFR1 (Fig S3E). These data suggest that association between TNFR1 cytoplasmic domains may act to stabilize TNFR1 clusters. However, time-lapse analysis of TNFR1 cluster movement at the membrane demonstrated that cells pre-treated with MβCD failed to increase speed in response to TNFα binding (Fig 3F). These data suggest that cholesterol-rich microdomains may not tether TNFR1 clusters, but rather potentially are required to promote interactions with other molecules within the membrane and induce subsequent signaling responses. To test this hypothesis, we analyzed activation of p65 (a subunit of the NFκB complex), p38 and JNK as the key mediators of downstream signaling from active TNFR1 by western blot. Treatment of cells with MβCD had no effect on activation of p65 in response to TNFα, but relative activation of both p38 and JNK were both significantly reduced compared to DMSO treated controls, as previously reported in non-adherent macrophages (17) (Fig 3G). Our combined data suggests that TNFR1 in adherent cells forms pre-assembled clusters, which require movement within the membrane in order to trigger specific downstream signals.

TNFR1 cluster movement correlates with ligand-receptor interaction number and signaling

In order to further define whether movement of TNFR1 clusters could be controlled by ligand binding, we quantified cluster movement in response to treatment of cells with homo-trimeric TNFα or where S162T/Y163A mutations were introduced into one, two or all three TNFα copies (mB, mBC and mABC respectively). Analytical size exclusion chromatography (AnSEC) analysis of TNFR1:TNFα binding confirmed the expected stoichiometry of receptor-ligand interactions for the single (mB) or double (mBC) mutated TNFα compared to WT (Fig S4A-C). Analysis of time-lapse movies demonstrated that treatment of cells with WT and mB TNFα triggered TNFR1 cluster movement on the membrane, whereas mBC and mABC TNFα did not (Fig 4A). These data indicated that two TNFR1 receptors need to be engaged with ligand under these conditions to induce movement of clusters on the membrane. To determine whether altered cluster speed correlated with altered signaling (as seen in MβCD treated cells), we analyzed activation of p65, p38 and JNK in lysates from cells treated with WT or mutant homo-trimeric TNFα. Whereas mB and mBC TNFα induced equally strong p65 phosphorylation when compared to WT ligand, mBC TNFα stimulated reduced amounts of pp38 and pJNK (Fig 4B). Furthermore, mABC TNFα did not induce a signaling response in

any of the pathways analyzed (Fig 4B). To define the phenotypic effects of treatment with these forms of TNFα, we analyzed cytokine secretion using an ELISA-based array. We found that WT TNF promoted the secretion of MIP-1α, CD40L, CXCL11, and GM-CSF by Hela cells, but only some of these changes were stimulated by B or BC mutants (Fig S5A,B). However, the proliferation rates in cells treated with the different TNF forms was unchanged over 48 hours (Fig S5C), which suggested that altered cytokine release was not acting in an autocrine fashion to alter cell division. This data further agrees with the earlier data indicating that treatment with TNF does not induce apoptosis in these cells.

To determine whether loss of TNFR1 receptor movement and signaling in mBC TNFα treated cells was correlated with altered TNFR1 clustering, we performed FRET/FLIM analysis of WT TNFR1 homo-oligomerization. The data demonstrated that mBC TNFα induced significantly less TNFR1 clustering compared to mB ligand (Fig 4C), which suggests that TNFα binding to a single receptor was not sufficient to induce TNFR1 interactions that promote cluster movement. To confirm this, we used STORM to quantify the degree of TNFR1 nanoscale clustering under the same conditions. We observed a significant increase in localizations of TNFR1 within high density clusters in WT TNFα treated cells, but not those stimulated with mBC TNFα (Fig 4D). Together, this data demonstrates that the number of interactions between TNFR1 and TNF can alter local receptor interaction, which are necessary to activate distinct signaling pathways.

Once activated, TNFR1 can recruit a range of different molecular adaptors and kinases that contribute to differential functional endpoints. In order to further determine whether TNFR1 clustering and movement correlated with recruitment of specific proteins to the cytoplasmic domains of TNFR1, we performed co-IP's of TNFR1 with known binding partners of complex I and its associated downstream kinases. We found that the abundance of TRAF2, SODD, RIP and FADD in complex with TNFR1 were unchanged in cells following TNFα treatment, both for TNFR1-GFP and endogenous TNFR1 (Fig S5A,B), which suggests that these may exist as pre-formed assemblies in adherent cells. However, analysis of TNFR1 colocalization with the MAPK family member MEKK1 demonstrated that TNFα promoted a significant increase in association (Fig 4E). Moreover, this enhanced colocalization between TNFR1 and MEKK1 was not seen in cells pre-treated with MβCD or those treated with mBC TNFα (Fig 4E). This TNF-dependent association was not seen with MLK3 (also MAPKKK11), which co-localized with TNFR1 in all conditions, including cholesterol-depleted cells (Fig S6C). This data suggests that coupling between TNFR1 and MEKK1 correlates with TNFα-TNFR1 cluster movement in adherent cells and the differential activation of p38 and JNK (28).

TNFR1 undergoes an ectodomain conformational change in response to ligand binding

Our data showed that TNFR1 clusters require interactions with at least 2 binding sites on the TNFα trimer to induce movement, which correlated with MEKK1 binding and activation of p38 and JNK. However, the molecular changes within TNFR1 clusters regulating this movement and capture of MEKK1 remain unclear. We hypothesized that when two or more TNFα molecules bind TNFR1, this may induce a conformational change within the ectodomain that promotes TNFR1 movement and a full complement of signaling activation.

To test this in intact cells, we performed FRET/FLIM analysis to quantify the proximity of the extreme N-terminal region of TNFR1 to the plasma membrane. Given that we observed no difference in receptor movement or clustering in response to ligand-binding in WT TNFR1 and ΔCD TNFR1 expressing cells, we first analyzed the potential for TNFα to induce changes to WT or ΔCD TNFR1. FLIM analysis demonstrated a population TNFR1 was in proximity to the plasma membrane in unstimulated cells, with no differences between WT and ΔCD TNFR1 (Fig 5A). However, TNFα stimulation resulted in a significant increase in WT TNFR1 proximity to the plasma membrane, which was not seen in ΔCD TNFR1 (Fig 5A). These data suggest that ligand-binding may promote shortening of the ectodomain of WT TNFR1. To determine whether this altered conformation was dependent upon the number of TNFR1-TNFα contact sites, we performed the same experiments in cells stimulated with mBC TNFα. We found no change in FRET in these cells, which demonstrated that trimeric interactions between TNFR1 and ligand are required for close membrane association (Fig 5B). Together, these data suggest that ligand binding may induce a conformational change within the extracellular domains of TNFR1 clusters that promotes closer association with the plasma membrane.

Discussion

TNFR1 is a key receptor in cellular decision-making between growth and inflammation or death. A large body of work over the past three decades has documented the signaling modes that can be triggered downstream of ligand binding to TNFR1. However, the very early events that occur within TNFR1 oligomeric structures that dictate these signaling decisions have remained unclear. Moreover, TNFR1 networks are presumed to be the signaling-competent architecture; the current model for receptor activation suggests ligand binding drives receptor trimerization, triggering reorganization of the cytosolic domains and higher-ordered network formation (29). Through combining high-resolution imaging and analysis of signaling endpoints, we showed that TNFR1 assembles into discrete pre-formed clusters at the plasma membrane of adherent cells (summarized in Fig 5C). These clusters are unchanged in PLAD or putative dimerization mutants within the TNFR1 CRD1/2 domains but are less abundant following removal of the cytoplasmic domain. Although the PLAD domain is important in constitutive dimerization or oligomerization or TNFR1 (3, 4, 18), our data would suggest that larger-scale membrane assemblies of TNFR1 are less reliant on PLAD extracellular domain interactions. Instead, the association with cytoplasmic proteins through the presence of the death domain may play a more important role in this process. Using both FRET/FLIM and STORM analysis, we showed this proximity was further increased upon binding of TNFα to pre-formed clusters, without altering the overall size of the clusters. STORM can provide molecular mapping of molecules at the ~20nm scale and FRET enables detection of interactions below 10nm (30, 31). Whereas many molecular details of intact TNFR1 are well-described (32), the potential molecular distances within pre-formed or ligand-induced TNFR1 groups have not been previously analyzed in intact adherent cells. Our combined high-resolution imaging approaches have therefore provided insight into receptor proximity and potential conformational changes that correlate with signaling outputs.

Our data demonstrates that changes at both the cytoplasmic and extracellular domains of TNFR1 are required for the tight receptor associations that correlate downstream kinase activation and inflammatory cytokine production. The increased proximity of the TNFR1 N-terminal region to the plasma membrane that we observe here only occurs upon engagement with trimeric TNF that binds 2 or 3 receptors. This is coupled with an increased in proximity of the cytoplasmic tails and increased clustering within larger scale pre-formed membrane assemblies of TNFR1. Whilst the structural details that underpin these combined conformational changes remain to be defined, our data would suggest that TNFα engages at least two receptors, which promotes increased TNFR1 packing and flattening of the larger-scale TNFR1 cluster with respect to the plasma membrane. Although CRD1 is not required for ligand-binding, this domain instead may act to stabilize a conformation of CRD2 that is permissive for ligand-induced activation of TNFR1 (7, 33). In our membrane-proximal FRET experiments, the increased interaction would be predicted to be at the N-terminal portion of CRD1, suggesting CRD1 also undergoes a conformational change within the receptor molecule that may promote ligand-receptor stabilization and thus full activation.

Although biochemical crosslinking approaches suggest that TNFR1 is a pre-formed trimer (3), studies using mutated TNFR1 ligands don't support similar conclusions (34). Our FRET and STORM data would also suggest that TNFR1 is at minimum a pre-formed dimer, as ligand interactions between adjacent receptors within these pre-formed clusters appears to be sufficient to induce a larger-scale assemblies which correlate with receptor activation, as has been previously suggested by molecular modelling experiments (32). The pre-assembled receptor clusters through cytoplasmic domain interactions would provide spatial proximity sufficient to engage two ligands simultaneously, thus initiating rapid receptor movement and capture of specific signaling molecules. Our data further suggests that a single TNF-TNFR1 ligand interaction can be sufficient to induce activation of NFκB pathways, but not JNK and p38. Our data revealed that TNFR1 cluster movement strongly correlated with increased colocalization between TNFR1 and MEKK1, which can initiate p38 and JNK signaling following stimulation by ligand (28, 35). Whereas we did not explore activation of every potential TNFR1-dependent pathway in this study, our data implies that the changes we observed are not required to trigger IKK signal initiation, and further suggests that differential ligand binding or receptor proximity may provide means to fine-tune the signaling response in different physiological contexts. Notably, the data we present in this study focuses on the effects of soluble TNFα on adherent cells. However, TNFα is can also exist as a less well studied trimeric 26kDa membrane tethered form (mTNFα), which can elicit both shared and distinct bioactivities when compared to the 17kDa cleaved, soluble form (36). In contrast to soluble TNFα, mTNFα acts in a juxtacrine fashion through cell-cell contact, which may present the ligand to TNFR in a different conformation, as well as maintaining contact for a longer duration to initiate different signaling outcomes. Applying the approaches we present in the current study to analyze TNFR-mTNFα interactions in future may provide new insight into the shared and distinct modes of action of these cytokine family members.

Our data demonstrates that in adherent cells, pre-formed TNFR1 clusters do not depend on actin or microtubule cytoskeletons and do not localize to lipid rafts or caveoloae. Whereas B and T cell receptors require an intact underlying actin cytoskeletal to initiate and propagate

signaling in response to ligand binding (37, 38), our study suggests that the cytoskeleton may not be the key factor that enables TNFR1 activation under the conditions tested. Moreover, although biochemical fractionation experiments suggest that that TNFR1 resides in lipid rafts microdomains (27), these domains are not required for signaling to occur (16, 17). It remains unclear how the pre-formed TNFR1 clusters are established at the plasma membrane and whether additional factors or microdomains within the membrane contribute to cluster stability. However, our FRAP data showed no significant movement of receptors between clusters or internalization of TNFR1 with or without the presence of ligand. This suggests that associations between cytoplasmic domains of adjacent TNFR1 molecules transported to the membrane, and subsequent binding to adaptor proteins, may provide sufficient means to stabilize pre-formed receptor complexes. Our data also indicated that TNFR1 clusters moved within the membrane after TNF binding in adherent cells. This mobility within the membrane did require the presence of cholesterol as well as a minimum of two TNF molecules interacting with adjacent TNFR1 molecules. This suggests that TNFR1 needs to undergo additional conformational changes to increase receptor proximity, potentially at minimum as a dimer within a larger network, and this promotes cluster movement. Future studies will be aimed at defining the mechanisms that control this movement and how this relates to TNFR1 conformational changes. Our study provides insight into the assembly requirements on both sides of the plasma membrane that precedes TNFR1 receptor movement and subsequent initiation of JNK/p38 signaling cascades. In addition to demonstrating differential nanoscale TNFR1 clustering correlates with signaling outcomes, this approach to defining how TNFR1 behaves under different physiological conditions may help refine anti-TNF and -TNFR1 therapeutics for inflammatory disease.

Materials and methods

Antibodies and reagents.

Anti-TNFR1 antibody (Mab225) was from R&D systems. Anti-HA, anti-phosp65 (ser576), anti-p65, anti-phosJNK, anti-JNK, anti-phos-p38, anti-p38, anti-MLK3, anti-MEKK1, anti-RIP, anti-TRADD, anti-TRAF2 and anti-clathrin antibodies were from Cell Signaling Technology. Anti-Myc antibody (clone 9E10) was from Sigma-Aldrich. Anti-GFP antibody was from Roche. Anti-GFP chromobody conjugated to Alexa647 was from Chromotek. Anti-HSC70 and anti-TNFR1 (H5) were from Santa Cruz. Anti-SODD was from Novus Biologicals. Anti-mouse HRP and anti-rabbit-HRP were from DAKO, anti-mouse-568, anti-rabbit-568 and phalloidin-647 were all obtained from Invitrogen.

Plasmids

TNFR1-YFP, TNFR1ΔCD-YFP, TNFR1-R92Q-YFP and TNFR1-C52F-YFP were a kind gift from Richard Siegel (NIAMS/NIH, Bethesda, USA). GFP tagged versions of these constructs were generated by subcloning TNFR1 sequences into eGFP-N1 (Clontech). EmGFP and TagRFP tagged versions were generated by subcloning EmGFP or TagRFP into NheI and XbaI of GFP-N1 plasmid. EmGFP DNA was generated by PCR and then inserted into GFP-N1. TNFR1 Q17/K19/H34/D49 AAAA-EmGFP and TagRFP were generated by site directed mutagenesis using the following PCR primers.

Q17A for: 5'GAGATAGTGTGTGTCCCGCAGGAAAATATATCCAC 3',
Q17A rev: 5' GTGGATATATTTTCCTGCGGGACACACACTATCTC 3',
K19A for: 5' GTGTGTCCCCAAGGAGCATATATCCACCCTC 3',
K19A rev: 5' GAGGGTGGATATATGCTCCTTGGGGACACAC 3',
H34A for: 5' GATTTGCTGTACCAAGTGCGCCAAAGGAACCTACTTGTAC 3',
H34A rev: 5' GTACAAGTAGGTTCCTTTGGCGCACTTGGTACAGCAAATC 3',
D49A for: 5' CCCGGGGCAGGCTACGGACTGCAGG 3',
D49A rev: 5' ACGTCAGGCATCGGACGGGGCCCGG 3'.
Fused heterotrimeric human TNFα was designed such that three copies of the human gene (UniProt P01375) were cloned in tandem separated by Ser-Gly-Ser linkers. The first copy of TNFα encodes residues 77-233, whereas the second and third copy encodes residues 86-233. The construct was optimized for *E.coli* expression (GeneComposer™), synthesized (ATUM) and cloned into the arabinose-inducible expression vector pEMB54 adding a 6His-Smt3 tag to the N-terminus. Receptor binding mutants were generated by introducing mutations S162T, Y163A (P01375 numbering) into the second copy of TNF (mB), second and third copies of TNF (mBC) or all three copies of TNF (mABC) using the Quik Change II Site-Directed Mutagenesis Kit (Agilent, Santa Clara, CA).

TNFα protein expression and purification

E.coli TOP10 cells (Thermofisher) transformed with each of the expression constructs, were cultured in TB (+100ug/ml ampicillin) to an OD600 = 0.6, expression was induced by adding arabinose (0.1%) and cultures were incubated for a further 16 hours at 20^0C. Cells were harvested by centrifugation and stored at -80^0C. Cells were resuspended (1g in 4ml) in 25mM Tris-HCL pH8.0, 200mM NaCl, 0.02% CHAPS, 50mM L-arginine, 125U of Benzonaze® (Novagen), 100mg lysozyme and one cOmplete™ EDTA-free protease inhibitor tablet (Roche) and lysed by sonication. Insoluble material was removed by centrifugation and His tagged protein was captured from the soluble fraction by immobilised metal affinity chromatography (IMAC) (HiTrap Chelating HP, GE Healthcare) eluted with a 500mM imidazole step or gradient. The 6His-Smt tag was removed with Ubiquitin-like-specific protease 1 (Ulp-1) while dialyzing against 2 L of 25 mM Tris pH 8.0 and 200 mM NaCl overnight at 4^0C in 10kDa MWCO snakeskin dialysis tubing. Cleaved protein was further purified by a second IMAC step, followed by size exclusion chromatography (HiPrep 16/60 Sephacryl S-100 HR, GE Healthcare) in 10mM HEPES, pH7.5, 150mM NaCl.

Analytical Size Exclusion Chromatography

Wild type and mutant forms (mB & mBC) of fused trimer hTNFα were incubated for 1 hour at 22°C with hTNFR1 at 1.2, 2.2, 3.2 & 3.5 fold molar excess over fused trimer (final concentrations: hTNFR1 90μM, 165μM, 240μM & 375μM, hTNFα 75μM). Samples were subject to analytical size exclusion using HPLC. Injection volumes of 50ul were separated on a TSK G3000SW L × I.D. 30 cm × 7.5 mm column (10um particle size) pre equilibrated in 10 mM HEPES, pH 7.5, 150 mM NaCl.

Cell culture

HeLa cells were obtained from ATCC and maintained in DMEM containing 10% FCS supplemented with penicillin and streptomycin. TNFR1 knockdown HeLa (HeLa-SH3) were

generated using pSP-u6(n) plasmids containing shRNA targeting the 5'UTR of TNFR1 mRNA which were obtained from Creative Biogene (NY, USA) and were maintained in HeLa growth media supplemented with 1μg/ml puromycin. Normal human keratinocytes were cultured in keratinocyte serum-free medium media (Invitrogen) supplemented with penicillin and streptomycin. HT1080 were a gift from Dr Vicky Sanz-Moreno (King's College London, UK) and were maintained in DMEM containing 10% FCS supplemented with penicillin and streptomycin. The fibroblast cell lines NIH-3T3 were obtained from ATCC and were maintained in DMEM containing 10% FCS supplemented with penicillin and streptomycin.

Western blotting and Immunoprecipitation

$1x10^5$ HeLa per condition were cultured in normal growth media and lysed in 100ul sample buffer containing β-mercapto-ethanol at room temperature. Lysates were immediately subjected to SDS-PAGE and blotted using nitrocellulose membrane. Blots were blocked and probed using 3% BSA/TBS-0.1%tween or 3%milk/PBS-0.1%tween.

For IP experiments, HeLa were transfected with TRAF2-myc or HeLa-SH3 transfected with TNFR1-GFP and cultured for a further 24 hours before treatment with 10ng/ml TNFα and lysis in IP lysis buffer (pH7.4 50 mM Tris, 150 mM NaCl, 1 mM EDTA, 0.5% NP40, PI cocktail). Lysates were incubated with 5μl GFP-TRAP or myc-TRAP beads for 30min before washing the beads with 1 ml IP lysis buffer 3 times. Immunocomplexes were separated using SDS-PAGE and immunoblotted for specified proteins.

Cytokine array

HeLa cells were grown to 60% confluency in 6-well plates, media changed to Optimem (Gibco, UK) with or without the addition of noted scTNFα (10ng/ml) and jncubated for 8h. Media was then removed and assayed using the Human Cytokine Array Proteome Prolifer Array (R+D Systems, Abingdon, UK) according to manufacturers instructions. Samples were then analyzed for mean spot pixel intensity by densitometry and resulting data presented as fold change compared to untreated control samples.

Proliferation assays

HeLa cells were plated at $2.5x10^4$ cells per well in serum-free media and left overnight to adhere. 5 wells per condition were then incubated serum-free media with no treatment or containing 10ng/ml WT or mutant TNF. Cells were placed into the incubator and fixed at either 24 or 48hours after treatment, followed by DAPI staining and imaging on an EVOS2-FL fluorescent microscope (Thermofisher, UK). Tile scans of every well were reconstructed in FIJI and nuclear counts per well calculated for each time point.

Sample preparation for confocal and TIRF microscopy

HeLa cells cultured on fibronectin coated 13mm coverslips were washed with PBS, fixed with 4% PFA in PBS for 10min. For detection of intracellular proteins cells were also permeabilized with 0.2% TritonX-100 for 10min before antibody incubation. Cells were incubated with primary antibodies for 2hours and appropriate secondary antibodies conjugated to alexafluor-568 or alexafluor-647 and Phalloidin conjugated to Alexafluor 568 or 647 for 1hour. Cells were mounted onto slides using Immunofluore (ICN).

For TIRF analysis, HeLa cells cultured in fibronectin coated 8 well glass bottomed chambers (Ibidi) were washed with PBS, fixed with 4% PFA in PBS for 10min. For detection of intracellular proteins cells were also permeabilized with 0.2% TritonX-100 for 10min before antibody incubation. Cells were incubated with primary antibodies for 2hours and appropriate secondary antibodies conjugated to alexafluor-488 or alexafluor-568. For TNF546 labelling, TNFR1-GFP transfected SH3 were incubated on ice for 20min with 10ng/ml TNF-546 in PBS before fixation with 4% PFA. TIRF images were acquired in PBS using a Nikon A1R microscopy with TIRF capability using a CFI Apo TIRF 60X Oil 1.48NA objective (Nikon) and cooled CCD camera (Hamamatsu).

Analysis of fixed TIRF images

TIRF images were analyzed for colocalization of TNFR1-GFP puncta and indicated proteins using JACoP plugin in FIJI (imagej.nih.gov/ij/plugins/track/jacop.html). Briefly corresponding green and red images were thresholded using the JACoP plugin to select membrane-associated punctae. Colocalization was then analyzed using Manders and plotted as mean values across at least 20 images per condition.

Time lapse TIRF microscopy and image analysis

For live tracking of TNFR1EmGFP clusters HeLa transfected with TNFR1-EmGFP were cultured in 8 well glass bottomed chambers (Ibidi) in imaging media supplemented with 25 mM HEPES. Images were acquired using a Nikon A1R microscopy with TIRF capability using a CFI Apo TIRF 60X Oil 1.48NA objective (Nikon). Temperature in the chamber was controlled to 37^{o}C using an environmental chamber and control unit (Okolab). Cells were then imaged every 30 seconds using 488 nm laser excitation with PFS activated. All images were saved as .nd2 files and analyzed using the trackmate Plugin (ImageJ). A Python script was written in-house to analysis the relationship between cluster area and speed of movement in the live cell TIRF microscopy data. To segment the images, we followed a similar approach to that described in (39) and applied wavelet filtering followed by watershed segmentation to identify the clusters. After segmentation the centroid position and area of each cluster can be determined. The cluster centroids were tracked using a Python implementation of the particle tracking algorithm first developed in (40) (https://zenodo.org/record/34028, 10.5281/zenodo.34028). Tracks with a minimum length of 10 frames were retained and their mean square displacement was calculated to allow determination of the cluster diffusion coefficient.

FRET/FLIM

For FRET experiments fibronectin coated 8 well glass bottomed chambers of HeLa-SH3 transfected with TNFR1-EmGFP and TNFR1-TagRFP plasmids were treated with 10ng/ml TNFα for 5min before fixation with 4% PFA and treatment with 0.1% triton X-100 and then 1mg/ml sodium borohydride. FLIM was used to measure FRET between EmGFP and TagRFP, which allows the determination of spatial protein interactions. Time domain FLIM was performed with a multifocal multiphoton FLIM microscope (MM-FLIM) system as described previously (41). In brief, light generated from a Chameleon Ultra II Ti:Sapphire laser source (Coherent Inc.) is coupled with a spatial light modulator (SLM) to generate a uniform 8 × 8 array of beamlets. This beamlet array is then relayed through a set of galvanometer scanners (providing x–y raster scanning capability) onto the back-pupil plane of a 40 × 1.3 N.A. Plan

Fluor oil objective (Nikon) where it is projected onto the sample. The two-photon generated fluorescence is collected and de-scanned where it is directed with a dichroic mirror and focused onto the Megaframe SPAD array using a 10 × 0.3 N.A. Plan Fluor air objective (Nikon). For each individual image acquisition, the system processed 64 × 64 data points for 8 × 8 detectors producing 512 × 512 pixel images. Lifetime data was acquired operating the Megaframe camera in TCPSC mode. In TCSPC mode, on-pixel TDCs generate raw time-correlated data, which are stored and then post-processed offline to generate an image. Once processed, these data are saved and then subsequently analyzed using TRI2 lifetime analysis software.

For FRET experiments measuring TNFR1 ECD conformational change fibronectin coated glass coverslips of HeLa-Sh3 transfected with HA-TNFR1 were treated with 10ng/ml TNFα for 5min before fixation with 4% PFA. Cells were blocked with 5% BSA-PBS then immunostained with anti-HA antibody (Cell Signaling) diluted 1in800 in 5% BSA-PBS followed by a Fab fragment directly conjugated to Alexafluo-488 secondary antibody diluted 1 in1000 in 1% BSA-PBS, without cell permeabilization. Coverslips were mounted using immunofluor. Time domain FLIM was performed with a multiphoton microscope system (Ti Eclipse microscope; Nikon) described in detail previously (42). Fluorescence lifetime imaging capability was provided by time-correlated single-photon counting electronics (SPC-830) on DCC-100 control (both Becker & Hickl). A 40× objective was used throughout (Plan Fluor N.A. 1.3; DIC H, WD 0.2; Nikon), and data were collected at 515 ± 20 nm through a bandpass filter. Acquisition times of the order of 250 s at a low 900-nm excitation laser power (MaiTai, DeepSee; Spectra-Physics) were used to achieve sufficient photon statistics for fitting, while avoiding either pulse pile up or photobleaching. Corresponding widefield fluorescent images were acquired for the acceptor (DHPE-TexasRed) channel (DS-Qi1Mc camera; Nikon). Lifetime raw data were analyzed with TRI2 software (Paul Barber) and histogram data are plotted as mean FRET efficiency from at least 30 cells per sample over three experiments. Alexa fluor 488 has been previously shown to fit to a biexponential lifetime with the longer lifetime (43). Thus, a bi-exponential fluorescence model was used to fit the data using in-house exponential fitting software (TRI2) utilizing a Levenberg-Marquardt algorithm, with the larger value interpreted as that of the Alexa 488 dye lifetime. Average lifetimes were calculated from the mean of all pixels measured within each image/cell and pooled from multiple experiments for statistical analysis. All graphs are plotted as mean FRET efficiency from >30 cells in total pooled from at least three independent experiments. Lifetime images of exemplary cells are presented using a pseudo-color scale whereby blue depicts normal Alexa 488 lifetime (*i.e.* no FRET) and red depicts reduced Alexa 488 lifetime (areas of high FRET). Analysis of variance was used to test statistical significance between different populations of data.

STORM analysis

For dSTORM experiments, fibronectin coated glass bottomed dishes of HeLa TNFR1 knockdown cells transfected with TNFR1-EmGFP and TNFR1-TagRFP plasmids were treated with 10ng/ml TNFα for 5min before fixation with 4% PFA and treatment with 0.1% triton X-100. Cells were then blocked with 5% BSA-PBS containing 0.2% Tween for 60min at room temperature before incubation with anti-GFP chromobody coupled to Alexa647 diluted 1 in 800 in 5% BSA-PBST for a further 60min. Cells were then washed 3 times with PBST and 3

times with PBS to remove residual antibody. Samples were then placed in STORM imaging buffer (Glucose oxidase, catalase, 1M MEA) prior to imaging. STORM measurements were performed on a customized STORM microscope, built around a DMi8 Microscope body and 'SuMo' passively stabilized stage (Leica-microsystems GMBH). In this system the 1.43 160X objective (Leica-microsystems GMBH) is mounted to the underside of the stage through a piezo drive (PI). Diode lasers of 638nm (Vortran), 561nm (Oxxius) 473nm (Dragon Laser) and 405nm (Vortran) as appropriate were depolarized through optic fibers, combined, apertured and expanded to pass through the objective and provide TIRF illumination. The TIRF beam reflected back through the objective was picked off with a half mirror and imaged on a 128 photo-diode micro array (RS). The signal was digitized and centroided by a micro-controller (Arduino). Focus drift caused displacement of the reflected beam on the array. This drift was monitored and corrected for using the piezo drive. Fluorescence was split according to wavelength by an image splitter (Photometrics Dual-view) and imaged side by side on a fast EMCCD camera (Photometrics Evolve). For GFP the filter window used was 500-530nm (the 'green' channel) and for Alexa647 it was 660-695nm (the 'red' channel). This was achieved with a multi-line major dichroic and emission filter set, beam-splitter and interference filters (Semrock). Low intensity 473nm light was used to excite the GFP while high intensity (ca 7KW/cm2) exited the Alexa647. Acquisitions consisted of 10,000 10ms frames. 'Snapshots' of the cluster positions in the 'green' channel were taken with a single 1s exposure frame just prior to acquisition (or alternatively made from integrating the first 100 frames of the acquisition). Acquired data were saved as tiff files and processed in Image J using the Thunderstorm plugin. The resulting localization tables were then imported into cluster density software.

Cluster analysis

Acquired data were saved TIFF files and processed in Image J using the Thunderstorm plugin (44). The localization tables were post-processed to retain only high-quality localizations and to remove background. Localizations were filtered to retain those with a determined precision less than 30nm and repeated localizations were merged using a maximum radius of 20nmX and 5 Y maximum off frames. The filtered localizations were grouped into clusters based on the local density. This was done by first forming Voronoi diagrams as in (45) and (46) and subsequently analyzing the local localization density using software written in-house using the Python programming language. The Voronoi diagram or tessellation was formed by partitioning the field-of-view into polygons, where there is exactly one polygon for each localization, such that any point within a polygon is closer to the localization than to any other point. The area of each polygon is then a direct indicator of the local density of each localization – polygons have small areas in dense regions. Clusters were defined by measuring the area of every polygon and retaining neighboring polygons where the area is smaller than a pre-set threshold and where the number of localizations within the region exceeds a minimum occupancy. The area threshold was determined as in (46) by comparing the experimental data with a simulated spatially random distribution of points with the same average density as the experimental data. Monte Carlo simulations were used to produce an average probability distribution of polygon sizes for the spatially random simulated data and this is compared with the distribution of polygon sizes in the experimental data. The intersection of the two distributions was used as a first pass automatic threshold to form a set of clusters from the experimental data. The retained localizations were then clustered a

second time with a more stringent density threshold to cluster any small, dense sub-regions of the first-pass clusters.

Statistical analysis
Data were analyzed using Prism software (Graphpad).

Supplementary Materials
Fig. S1. TNFR1 clusters occur in multiple adherent cell types
Fig. S2. TNFR1 molecules increase homotypic associations in response to ligand binding
Fig. S3. TNFR1 clusters do not require membrane microdomains or cytoskeleton for assembly
Fig. S4. Analytical size exclusion chromatography (AnSEC) analysis of titration of TNFR1 with scTNFα
Fig. S5. Differential cytokine release in response to mutant scTNFα binding
Fig. S6. TNFR1 clusters do not change association with complex I proteins or MLK3 in response to TNF

References and Notes

1. Kalliolias, G. D., and L. B. Ivashkiv. 2016. TNF biology, pathogenic mechanisms and emerging therapeutic strategies. *Nat Rev Rheumatol* 12: 49-62.
2. Idriss, H. T., and J. H. Naismith. 2000. TNF alpha and the TNF receptor superfamily: structure-function relationship(s). *Microsc Res Tech* 50: 184-195.
3. Chan, F. K., H. J. Chun, L. Zheng, R. M. Siegel, K. L. Bui, and M. J. Lenardo. 2000. A domain in TNF receptors that mediates ligand-independent receptor assembly and signaling. *Science* 288: 2351-2354.
4. Deng, G. M., L. Zheng, F. K. Chan, and M. Lenardo. 2005. Amelioration of inflammatory arthritis by targeting the pre-ligand assembly domain of tumor necrosis factor receptors. *Nat Med* 11: 1066-1072.
5. McDermott, M. F., I. Aksentijevich, J. Galon, E. M. McDermott, B. W. Ogunkolade, M. Centola, E. Mansfield, M. Gadina, L. Karenko, T. Pettersson, J. McCarthy, D. M. Frucht, M. Aringer, Y. Torosyan, A. M. Teppo, M. Wilson, H. M. Karaarslan, Y. Wan, I. Todd, G. Wood, R. Schlimgen, T. R. Kumarajeewa, S. M. Cooper, J. P. Vella, C. I. Amos, J. Mulley, K. A. Quane, M. G. Molloy, A. Ranki, R. J. Powell, G. A. Hitman, J. J. O'Shea, and D. L. Kastner. 1999. Germline mutations in the extracellular domains of the 55 kDa TNF receptor, TNFR1, define a family of dominantly inherited autoinflammatory syndromes. *Cell* 97: 133-144.
6. Galon, J., I. Aksentijevich, M. F. McDermott, J. J. O'Shea, and D. L. Kastner. 2000. TNFRSF1A mutations and autoinflammatory syndromes. *Curr Opin Immunol* 12: 479-486.
7. Banner, D. W., A. D'Arcy, W. Janes, R. Gentz, H. J. Schoenfeld, C. Broger, H. Loetscher, and W. Lesslauer. 1993. Crystal structure of the soluble human 55 kd TNF receptor-human TNF beta complex: implications for TNF receptor activation. *Cell* 73: 431-445.

8. Naismith, J. H., T. Q. Devine, B. J. Brandhuber, and S. R. Sprang. 1995. Crystallographic evidence for dimerization of unliganded tumor necrosis factor receptor. *J Biol Chem* 270: 13303-13307.
9. Mukai, Y., T. Nakamura, M. Yoshikawa, Y. Yoshioka, S. Tsunoda, S. Nakagawa, Y. Yamagata, and Y. Tsutsumi. 2010. Solution of the structure of the TNF-TNFR2 complex. *Sci Signal* 3: ra83.
10. Cabal-Hierro, L., and P. S. Lazo. 2012. Signal transduction by tumor necrosis factor receptors. *Cell Signal* 24: 1297-1305.
11. Blackwell, K., L. Zhang, L. M. Workman, A. T. Ting, K. Iwai, and H. Habelhah. 2013. Two coordinated mechanisms underlie tumor necrosis factor alpha-induced immediate and delayed IkappaB kinase activation. *Mol Cell Biol* 33: 1901-1915.
12. Haas, T. L., C. H. Emmerich, B. Gerlach, A. C. Schmukle, S. M. Cordier, E. Rieser, R. Feltham, J. Vince, U. Warnken, T. Wenger, R. Koschny, D. Komander, J. Silke, and H. Walczak. 2009. Recruitment of the linear ubiquitin chain assembly complex stabilizes the TNF-R1 signaling complex and is required for TNF-mediated gene induction. *Mol Cell* 36: 831-844.
13. Geng, J., Y. Ito, L. Shi, P. Amin, J. Chu, A. T. Ouchida, A. K. Mookhtiar, H. Zhao, D. Xu, B. Shan, A. Najafov, G. Gao, S. Akira, and J. Yuan. 2017. Regulation of RIPK1 activation by TAK1-mediated phosphorylation dictates apoptosis and necroptosis. *Nat Commun* 8: 359.
14. Heidbreder, M., C. Zander, S. Malkusch, D. Widera, B. Kaltschmidt, C. Kaltschmidt, D. Nair, D. Choquet, J. B. Sibarita, and M. Heilemann. 2012. TNF-alpha influences the lateral dynamics of TNF receptor I in living cells. *Biochim Biophys Acta* 1823: 1984-1989.
15. Poggi, M., I. Kara, J. M. Brunel, J. F. Landrier, R. Govers, B. Bonardo, R. Fluhrer, C. Haass, M. C. Alessi, and F. Peiretti. 2013. Palmitoylation of TNF alpha is involved in the regulation of TNF receptor 1 signalling. *Biochim Biophys Acta* 1833: 602-612.
16. Hunter, I., and G. F. Nixon. 2006. Spatial compartmentalization of tumor necrosis factor (TNF) receptor 1-dependent signaling pathways in human airway smooth muscle cells. Lipid rafts are essential for TNF-alpha-mediated activation of RhoA but dispensable for the activation of the NF-kappaB and MAPK pathways. *J Biol Chem* 281: 34705-34715.
17. Doan, J. E., D. A. Windmiller, and D. W. Riches. 2004. Differential regulation of TNF-R1 signaling: lipid raft dependency of p42mapk/erk2 activation, but not NF-kappaB activation. *J Immunol* 172: 7654-7660.
18. Lobito, A. A., F. C. Kimberley, J. R. Muppidi, H. Komarow, A. J. Jackson, K. M. Hull, D. L. Kastner, G. R. Screaton, and R. M. Siegel. 2006. Abnormal disulfide-linked oligomerization results in ER retention and altered signaling by TNFR1 mutants in TNFR1-associated periodic fever syndrome (TRAPS). *Blood* 108: 1320-1327.
19. Lo, C. H., N. Vunnam, A. K. Lewis, T. L. Chiu, B. E. Brummel, T. M. Schaaf, B. D. Grant, P. Bawaskar, D. D. Thomas, and J. N. Sachs. 2017. An Innovative High-Throughput Screening Approach for Discovery of Small Molecules That Inhibit TNF Receptors. *SLAS Discov* 22: 950-961.
20. Marguet, D., P. F. Lenne, H. Rigneault, and H. T. He. 2006. Dynamics in the plasma membrane: how to combine fluidity and order. *EMBO J* 25: 3446-3457.

21. Choquet, D., and A. Triller. 2003. The role of receptor diffusion in the organization of the postsynaptic membrane. *Nat Rev Neurosci* 4: 251-265.
22. Schneider-Brachert, W., V. Tchikov, J. Neumeyer, M. Jakob, S. Winoto-Morbach, J. Held-Feindt, M. Heinrich, O. Merkel, M. Ehrenschwender, D. Adam, R. Mentlein, D. Kabelitz, and S. Schutze. 2004. Compartmentalization of TNF receptor 1 signaling: internalized TNF receptosomes as death signaling vesicles. *Immunity* 21: 415-428.
23. Higuchi, M., and B. B. Aggarwal. 1994. TNF induces internalization of the p60 receptor and shedding of the p80 receptor. *J Immunol* 152: 3550-3558.
24. Watanabe, N., H. Kuriyama, H. Sone, H. Neda, N. Yamauchi, M. Maeda, and Y. Niitsu. 1988. Continuous internalization of tumor necrosis factor receptors in a human myosarcoma cell line. *J Biol Chem* 263: 10262-10266.
25. D'Alessio, A., B. Esposito, C. Giampietri, E. Ziparo, J. S. Pober, and A. Filippini. 2012. Plasma membrane microdomains regulate TACE-dependent TNFR1 shedding in human endothelial cells. *J Cell Mol Med* 16: 627-636.
26. Hawari, F. I., F. N. Rouhani, X. Cui, Z. X. Yu, C. Buckley, M. Kaler, and S. J. Levine. 2004. Release of full-length 55-kDa TNF receptor 1 in exosome-like vesicles: a mechanism for generation of soluble cytokine receptors. *Proc Natl Acad Sci U S A* 101: 1297-1302.
27. Legler, D. F., O. Micheau, M. A. Doucey, J. Tschopp, and C. Bron. 2003. Recruitment of TNF receptor 1 to lipid rafts is essential for TNFalpha-mediated NF-kappaB activation. *Immunity* 18: 655-664.
28. Sun, B. K., J. H. Kim, H. N. Nguyen, S. Oh, S. Y. Kim, S. Choi, H. J. Choi, Y. J. Lee, and J. J. Song. 2011. MEKK1/MEKK4 are responsible for TRAIL-induced JNK/p38 phosphorylation. *Oncol Rep* 25: 537-544.
29. Peltzer, N., M. Darding, and H. Walczak. 2016. Holding RIPK1 on the Ubiquitin Leash in TNFR1 Signaling. *Trends Cell Biol* 26: 445-461.
30. Fricke, F., M. S. Dietz, and M. Heilemann. 2015. Single-molecule methods to study membrane receptor oligomerization. *Chemphyschem* 16: 713-721.
31. Sieben, C., K. M. Douglass, P. Guichard, and S. Manley. 2018. Super-resolution microscopy to decipher multi-molecular assemblies. *Curr Opin Struct Biol* 49: 169-176.
32. Lewis, A. K., C. C. Valley, and J. N. Sachs. 2012. TNFR1 signaling is associated with backbone conformational changes of receptor dimers consistent with overactivation in the R92Q TRAPS mutant. *Biochemistry* 51: 6545-6555.
33. Branschadel, M., A. Aird, A. Zappe, C. Tietz, A. Krippner-Heidenreich, and P. Scheurich. 2010. Dual function of cysteine rich domain (CRD) 1 of TNF receptor type 1: conformational stabilization of CRD2 and control of receptor responsiveness. *Cell Signal* 22: 404-414.
34. Boschert, V., A. Krippner-Heidenreich, M. Branschadel, J. Tepperink, A. Aird, and P. Scheurich. 2010. Single chain TNF derivatives with individually mutated receptor binding sites reveal differential stoichiometry of ligand receptor complex formation for TNFR1 and TNFR2. *Cell Signal* 22: 1088-1096.
35. Hu, W. H., H. Johnson, and H. B. Shu. 1999. Tumor necrosis factor-related apoptosis-inducing ligand receptors signal NF-kappaB and JNK activation and apoptosis through distinct pathways. *J Biol Chem* 274: 30603-30610.
36. Wallach, D. 2018. The Tumor Necrosis Factor Family: Family Conventions and Private Idiosyncrasies. *Cold Spring Harb Perspect Biol* 10.

37. Song, W., C. Liu, and A. Upadhyaya. 2014. The pivotal position of the actin cytoskeleton in the initiation and regulation of B cell receptor activation. *Biochim Biophys Acta* 1838: 569-578.
38. Thauland, T. J., K. H. Hu, M. A. Bruce, and M. J. Butte. 2017. Cytoskeletal adaptivity regulates T cell receptor signaling. *Sci Signal* 10.
39. Izeddin, I., J. Boulanger, V. Racine, C. G. Specht, A. Kechkar, D. Nair, A. Triller, D. Choquet, M. Dahan, and J. B. Sibarita. 2012. Wavelet analysis for single molecule localization microscopy. *Opt Express* 20: 2081-2095.
40. Crocker, J. C., and D. G. Grier. 1996. Methods of digital video microscopy for colloidal studies. *J Colloid Interf Sci* 179: 298-310.
41. Poland, S. P., N. Krstajic, J. Monypenny, S. Coelho, D. Tyndall, R. J. Walker, V. Devauges, J. Richardson, N. Dutton, P. Barber, D. D. Li, K. Suhling, T. Ng, R. K. Henderson, and S. M. Ameer-Beg. 2015. A high speed multifocal multiphoton fluorescence lifetime imaging microscope for live-cell FRET imaging. *Biomed Opt Express* 6: 277-296.
42. Randall, T. S., Y. Y. Yip, D. J. Wallock-Richards, K. Pfisterer, A. Sanger, W. Ficek, R. A. Steiner, A. J. Beavil, M. Parsons, and M. P. Dodding. 2017. A small-molecule activator of kinesin-1 drives remodeling of the microtubule network. *Proc Natl Acad Sci U S A* 114: 13738-13743.
43. Waterhouse, B. R., M. Gijsen, P. R. Barber, I. D. Tullis, B. Vojnovic, and A. Kong. 2011. Assessment of EGFR/HER2 dimerization by FRET-FLIM utilizing Alexa-conjugated secondary antibodies in relation to targeted therapies in cancers. *Oncotarget* 2: 728-736.
44. Ovesny, M., P. Krizek, J. Borkovec, Z. Svindrych, and G. M. Hagen. 2014. ThunderSTORM: a comprehensive ImageJ plug-in for PALM and STORM data analysis and super-resolution imaging. *Bioinformatics* 30: 2389-2390.
45. Andronov, L., I. Orlov, Y. Lutz, J. L. Vonesch, and B. P. Klaholz. 2016. ClusterViSu, a method for clustering of protein complexes by Voronoi tessellation in super-resolution microscopy. *Sci Rep* 6: 24084.
46. Levet, F., E. Hosy, A. Kechkar, C. Butler, A. Beghin, D. Choquet, and J. B. Sibarita. 2015. SR-Tesseler: a method to segment and quantify localization-based super-resolution microscopy data. *Nat Methods* 12: 1065-1071.

Acknowledgments: The authors thank Richard Siegel (NIH, USA) for TNFR1 plasmids. The authors also to thank Sanofi for their generous support and contributions to the study, David Fox III, Jameson Bullen and Rena Grice for design, production and characterization of the fused TNF protein and David Schubert and James O'Connell for their helpful contribution to discussions. The authors also gratefully acknowledge technical support from the Nikon Imaging Centre@King's. **Funding:** This work was funded by the King's Health Partners National Institute for Health Research (NIHR) Clinical Research Facility and NIHR Biomedical Research Centre based at Guy's and St. Thomas' National Health Service Foundation Trust, King's College London (to MP), the Biotechnology and Biological Sciences Research Council (BB/L015773/1 to MP and SC), the Medical Research Council (MR/K015664/1 to MP and SAB), and UCB Pharma. **Author contributions:** PEM and CP performed the experiments with input from MP and SAB, with assistance for FLIM and STORM experiments from JL and DRM/RJM respectively. SP built the FLIM system with assistance from SAB and provided data analysis input. DRM performed the cluster analysis

and assisted with STORM data analysis. The study was conceived by MP with input from AM, DM and SAB. All authors contributed to the final manuscript text. **Competing Interests:** AM and DM are employees of UCB Pharma and may hold stock and/or stock options. The other authors declare that they have no competing financial interests. **Data and materials availability:** All data needed to evaluate the conclusions in the paper are present in the paper or the Supplementary Materials.

Figure legends

Fig. 1. TNFR1 assembles into pre-formed clusters at the plasma membrane. (**A**) TIRFM microscopy analysis of TNFR1 cluster abundance in HeLa cells expressing TNFR1-GFP that were starved (untreated) or TNFα treated, as indicated. (**B**) TIRFM images of HeLa cells expressing WT TNFR1-GFP and specified mutants. (**C**) TIRF microscopy analysis of TNFR1 clustering in HeLa cells co-expressing TNFR1-GFP (green) and WT or mutant TNFR1-RFP (magenta). (**D**) FRET analysis by fluorescence lifetime of TNFR1 dimerization in cells expressing WT or ΔCD TNFR1-GFP alone (donor alone) or co-expressed with WT or ΔCD TNFR1-RFP treated with or without TNFα. All images (left) with are representative of 3 independent experiments. White lines (A to C) denote plasma membrane boundary. Scale bars, 10μm. All quantified data (right) are means ± SEM of 30 cells/condition pooled from all experiments. *P<0.01 and *** P<0.001 by 2-way ANOVA.

Fig. 2. TNFR1 increases nanoscale clustering in response to ligand binding. (**A**) Confocal microscopy of TNFR1-GFP and TNFR1-RFP expressing HeLa cells before and after photobleaching. Images (left, middle) are representative of 3 independent experiments. Quantified fluorescence recovery of TNFR1-GFP in clusters over time are means ± SEM of 15 cells from all experiments. (**B** to **F**) STORM analysis of GFP clusters in TNFR1-GFP expressing HeLa cells treated with TNFα, as indicated. Images (B) are representative of 3 independent experiments. Quantification of total GFP area (C), the percentage of GFP localized within high-density (D) or low-density (E) clusters, and the percentage of GFP-containing high-density clusters of total clusters (F) with median values ± upper and lower percentiles of at least 16 cells are pooled from all experiments. Scale bar, 10μm (A) or 1μm (B). **P<0.001 by Students two-tailed T-Test.

Fig. 3. TNFR1 clusters move on the membrane in response to ligand binding. (**A** and **B**) TIRFM analysis of TNFR1 clusters in HeLa cells expressing TNFR1-GFP that were TNFα treated, as indicated. Images (A, left) are representative of 3 independent experiments. White lines denote plasma membrane boundary and color scale indicates track position over time (black = time 0 and yellow = 10 mins). Quantified TNFR1-GFP cluster movement speed (A, right) data with medians ± quartile values of 30 cells/condition are from all experiments. Plots of TNFR1-GFP cluster diffusion co-efficient compared to cluster size (B, left) representative of 3 independent experiments and cluster area as function of frequency (B, right) in treated and untreated cells are means± SEM of 30 cells/condition pooled from 3 independent experiments . (**C**) Western blot for TNFR1 in biotin immunoprecipitates from lysates of surface biotinylated cells (input) incubated at 37^0C for the indicated times. Blots are representative of 5 independent experiments and quantification of internalized TNFR1 (below) are means± SEM. (**D**) Western blots for the indicated proteins in lysates of HeLa cells treated with Dynasore and TNFα for 15 or 30 mins, as indicated. Blots are representative of 3 independent experiments and quantification of p-p65 (below) are means± SEM. (**E**) TIRFM analysis of HeLa cells expressing TNFR1-GFP (green) and Cholera Toxin B subunit-A568 (magenta) in cells treated with DMSO or methyl-β-cyclodextran (MβCD). Images (left) are representative of 3 independent experiments. Quantified colocalization of TNFR1:CTxB are means± SEM of 30 cells/condition from all experiments. (**F**) TIRFM analysis of TNFR1 cluster

speed in starved (untreated) or TNFα treated HeLa cells pre-treated with MβCD for 10 minutes, as indicates. Data with medians ± quartile values of 30 cells are from 3 independent experiments. (**G**) Western blots for pp65, pp38, and pJNK in cells treated with TNFα and or MβCD as indicates. Blots (left) are representative of 5 independent experiments. Quantified band intensity values (right) are means ± SEM from all experiments. Scale bars, 10μm. *P<0.01 and ***P<0.001 by 2-way ANOVA.

Fig. 4. TNFR1 cluster movement requires TNFα binding to at least two adjacent TNFR1 molecules. (**A**) TIRFM analysis of TNFR1-GFP in HeLa cells treated with WT or mutant TNFα, as indicated. Representative color-coded tracks from 10-minute movies are shown. Images are representative of 3 independent experiments. White lines denote plasma membrane boundary and color scale indicates track position over time (black = time 0 and yellow = 10 mins). Quantified TNFR1-GFP cluster movement speed data with medians ± quartile values of 30 cells are from all experiments. (**B**) Western blots for pp65, pp38, and pJNK in HeLa cells treated with WT or mutant TNFα, as indicated. Blots (upper) are representative of 5 independent experiments. Quantified band intensity values (lower) are medians ± quartile values from all experiments. (**C**) FRET analysis in cells co-expressing WT TNFR1-GFP and WT TNFR1-RFP untreated or treated with mutant TNFα. Data are medians ± SEM of 30 cells from 3 independent experiments (**D**) STORM analysis of TNFR1 clusters from HeLacells treated with WT or mutant TNFα. Images are representative of 3 independent experiments. (**E**) TRIFM analysis of TNFR1 (green) and MEKK1 (magenta) in TNFR1-GFP HeLa cells treated with WT or mutBC TNFα. Images (upper) are representative of 3 independent experiments. White lines denote plasma membrane boundary. Colocalization co-efficient data are means ± SEM from all experiments. Scale bars, 10μm. *P<0.01, ** P<0.005, and *** P<0.001 by 2-way ANOVA.

Fig. 5. TNFR1 undergoes a conformational change in the ectodomain in response to TNFα binding. (**A**) FRET lifetime analysis of TNFR1 membrane proximity in HeLa cells expressing WT or ΔCD HA-TNFR1 that were treated with TNFα as indicated and stained for HA (green) and DHPE (blue). Images (left) are representative of 3 independent experiments. Quantified FRET efficiency data (right) are means ± SEM of 45 cells from all experiments. (**B**) FRET lifetime analysis of TNFR1 membrane proximity in XX cells expressing HA-TNFR1 that were treated with WT or mutant TNFα as indicated and stained for HA (green) and DHPE (blue). Images (left) are representative of 3 independent experiments. Quantified FRET efficiency data (right) are means ± SEM of 30 cells pooled from all experiments. (**C**) Model of potential TNFR1 ectodomain conformational changes under different ligand binding states. Scale bars, 10μm. *P<0.01, **P>0.005, and ***P<0.001 by two-tailed T-test (A) or 2-way ANOVA (B).

Figure 1

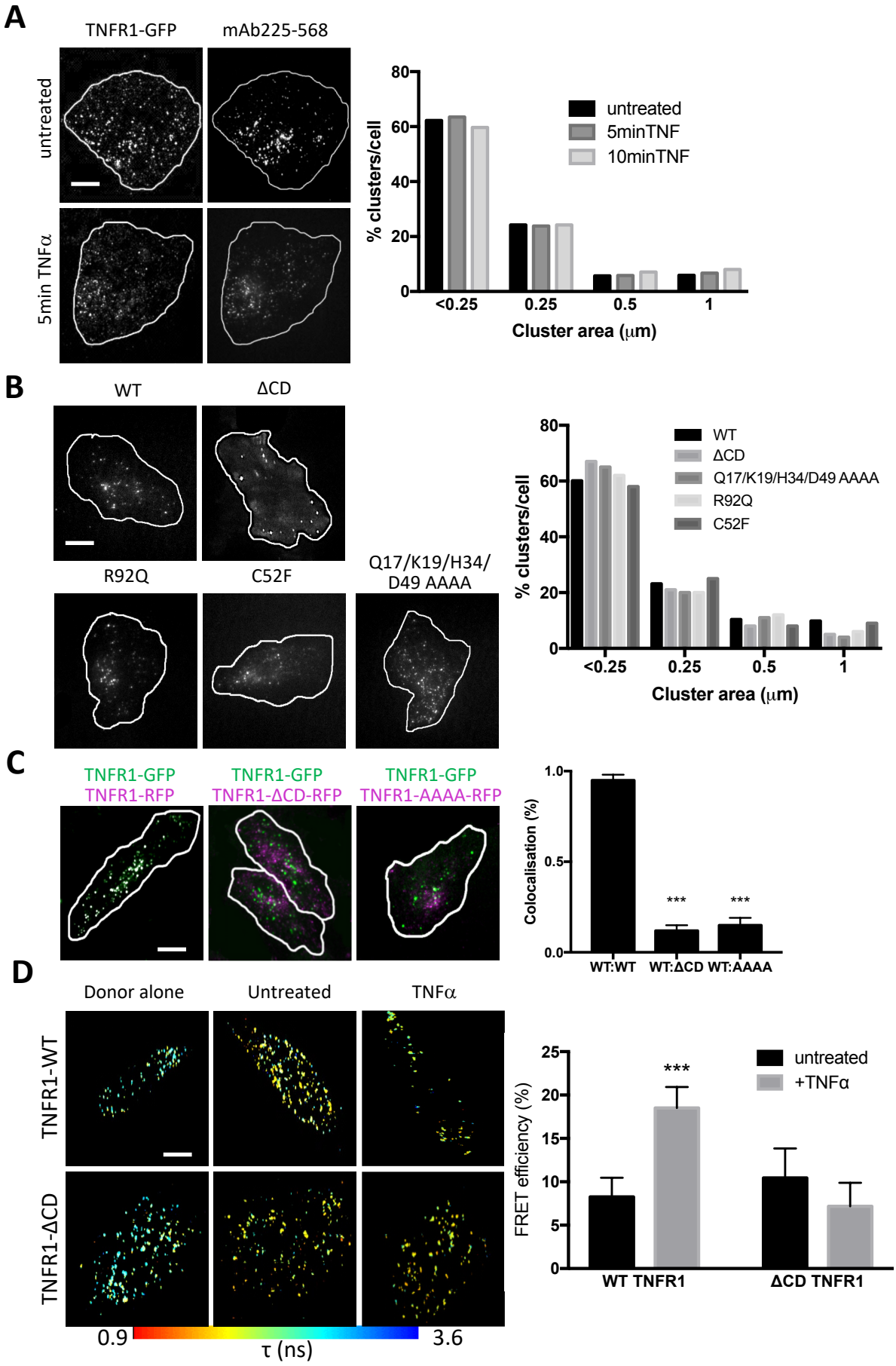
A
TNFR1-GFP
mAb225-568
untreated
5min TNFα
% clusters/cell
80
60
40
20
0
<0.25
0.25
0.5
1
Cluster area (μm)
untreated
5minTNF
10minTNF
B
WT
ΔCD
R92Q
C52F
Q17/K19/H34/
D49 AAAA
% clusters/cell
Cluster area (μm)
WT
ΔCD
Q17/K19/H34/D49 AAAA
R92Q
C52F
C
TNFR1-GFP
TNFR1-RFP
TNFR1-GFP
TNFR1-ΔCD-RFP
TNFR1-GFP
TNFR1-AAAA-RFP
Colocalisation (%)
1.0
0.5
0.0
***
***
WT:WT
WT:ΔCD
WT:AAAA
D
Donor alone
Untreated
TNFα
TNFR1-WT
TNFR1-ΔCD
0.9
τ (ns)
3.6
FRET efficiency (%)
25
20
15
10
5
0
***
untreated
+TNFα
WT TNFR1
ΔCD TNFR1

Figure 2

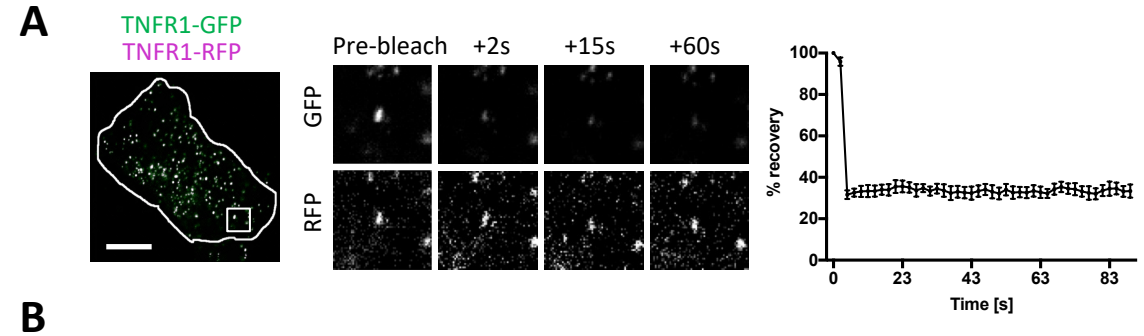
A
TNFR1-GFP
TNFR1-RFP
Pre-bleach
+2s
+15s
+60s
GFP
RFP
% recovery
Time [s]

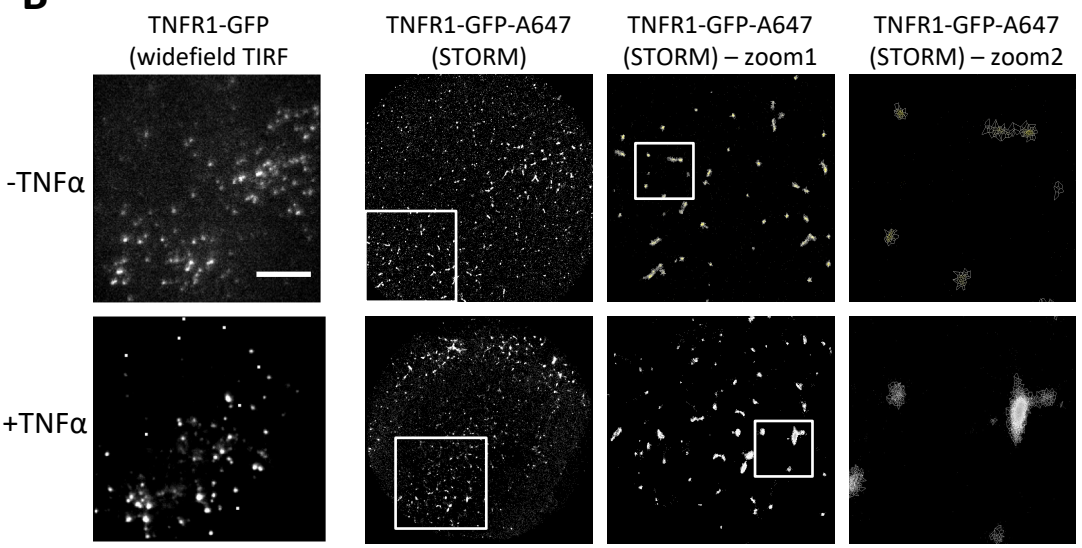
B
TNFR1-GFP (widefield TIRF)
TNFR1-GFP-A647 (STORM)
TNFR1-GFP-A647 (STORM) – zoom1
TNFR1-GFP-A647 (STORM) – zoom2
-TNFα
+TNFα

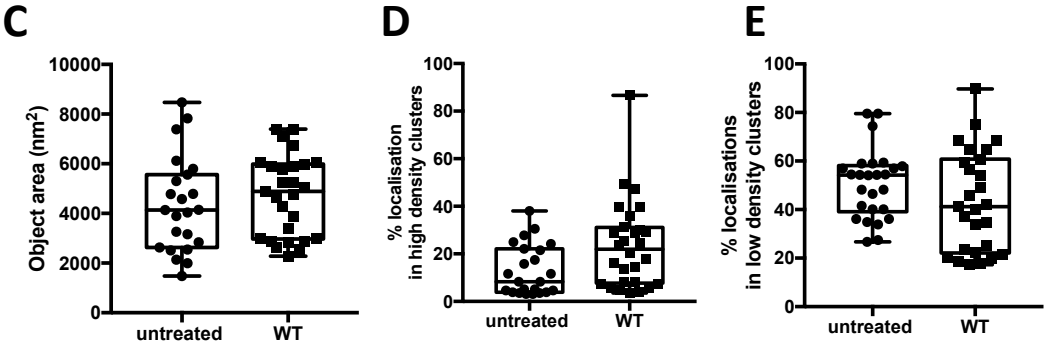
C
Object area (nm²)
untreated
WT
D
% localisation in high density clusters
untreated
WT
E
% localisations in low density clusters
untreated
WT

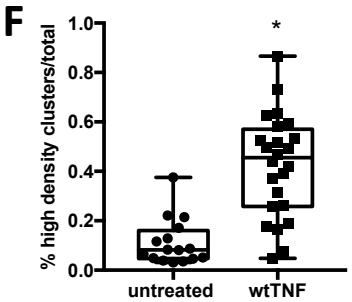
F
% high density clusters/total
*
untreated
wtTNF

Figure 3

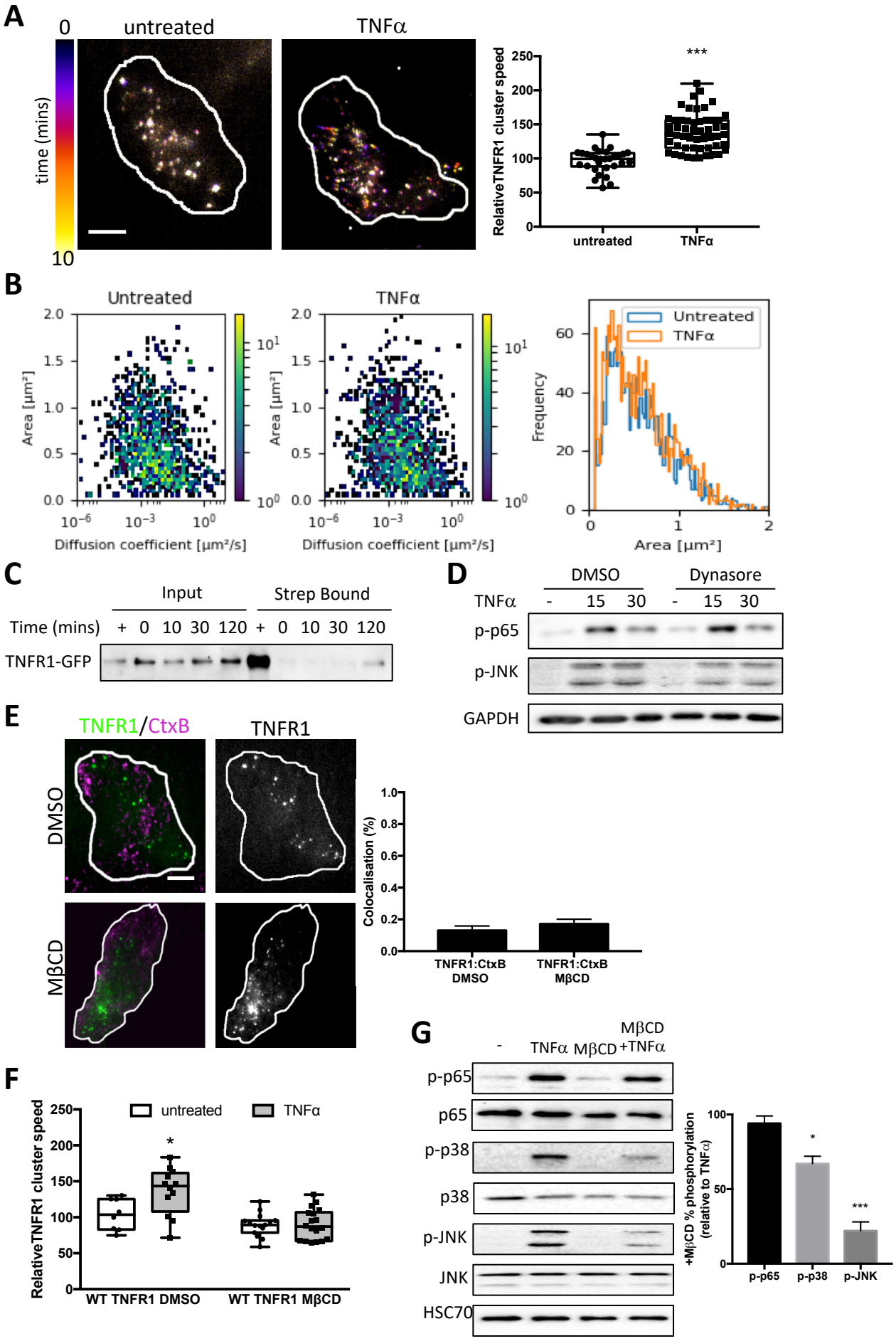
A
0
untreated
TNFα
time (mins)
10
RelativeTNFR1 cluster speed
***
untreated
TNFα
B
Untreated
TNFα
Area [μm²]
Diffusion coefficient [μm²/s]
Frequency
Area [μm²]
C
Input
Strep Bound
Time (mins) + 0 10 30 120 + 0 10 30 120
TNFR1-GFP
D
DMSO
Dynasore
TNFα - 15 30 - 15 30
p-p65
p-JNK
GAPDH
E
TNFR1/CtxB
TNFR1
DMSO
MβCD
Colocalisation (%)
TNFR1:CtxB DMSO
TNFR1:CtxB MβCD
F
untreated
TNFα
RelativeTNFR1 cluster speed
WT TNFR1 DMSO
WT TNFR1 MβCD
G
- TNFα MβCD MβCD +TNFα
p-p65
p65
p-p38
p38
p-JNK
JNK
HSC70
+MβCD % phosphorylation (relative to TNFα)
p-p65
p-p38
p-JNK

Figure 4

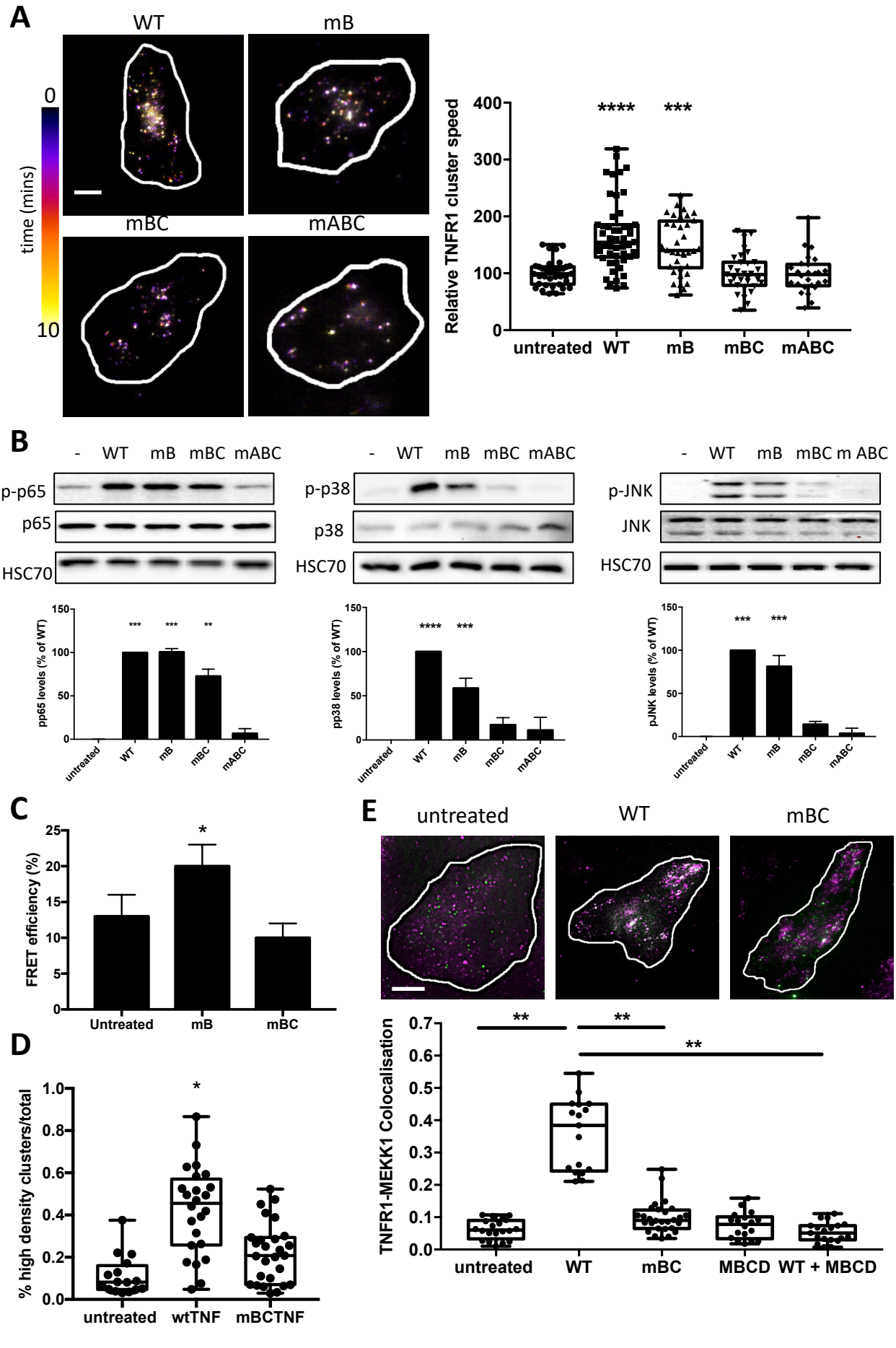
A
WT
mB
mBC
mABC
0
10
time (mins)
Relative TNFR1 cluster speed
untreated
WT
mB
mBC
mABC
B
p-p65
p65
HSC70
p-p38
p38
p-JNK
JNK
pp65 levels (% of WT)
pp38 levels (% of WT)
pJNK levels (% of WT)
C
FRET efficiency (%)
Untreated
mB
mBC
D
% high density clusters/total
untreated
wtTNF
mBCTNF
E
untreated
WT
mBC
TNFR1-MEKK1 Colocalisation
MBCD
WT + MBCD

Figure 5

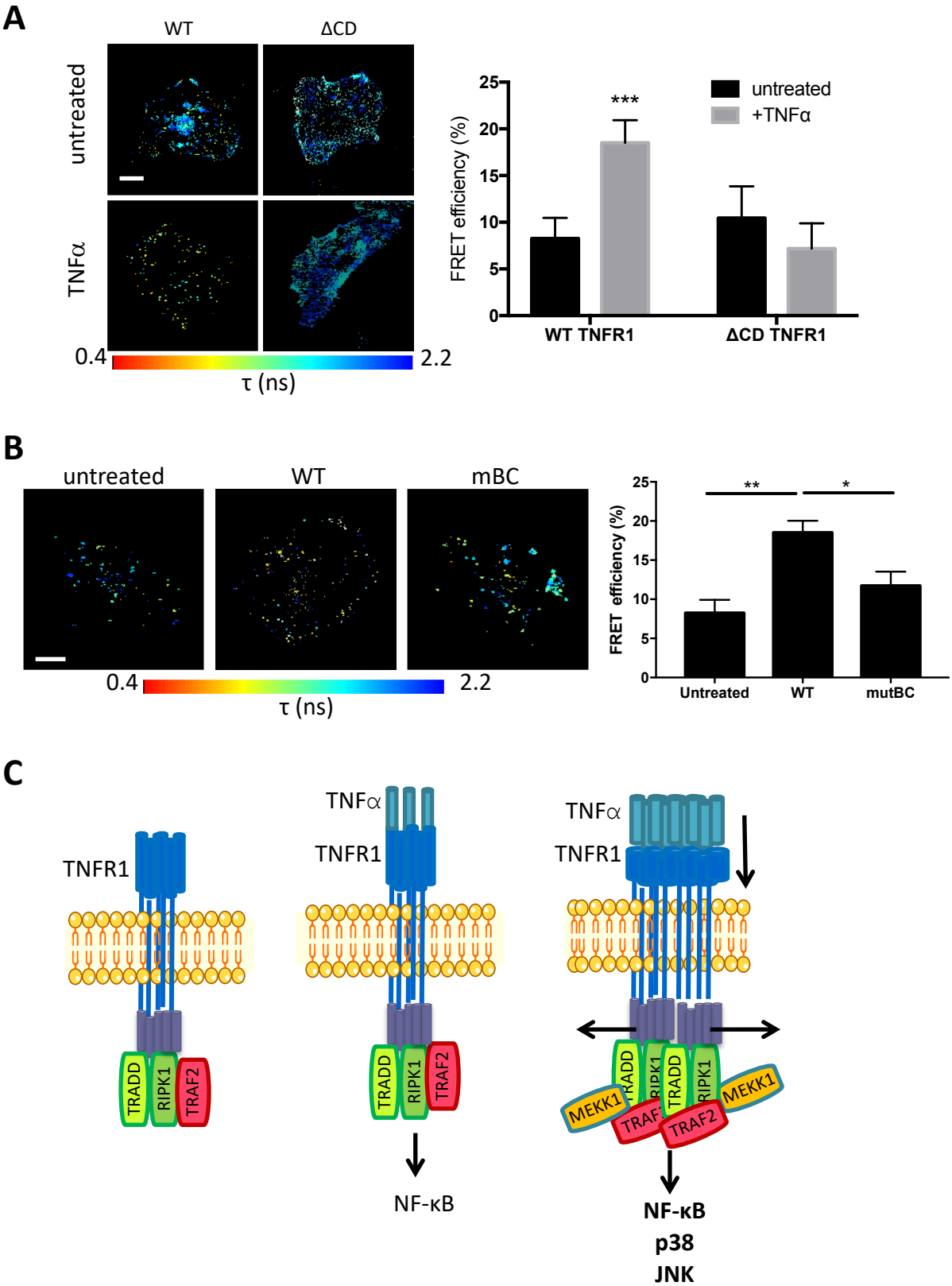
A
WT
ΔCD
untreated
TNFα
0.4
2.2
τ (ns)
FRET efficiency (%)
***
untreated
+TNFα
WT TNFR1
ΔCD TNFR1
B
untreated
WT
mBC
0.4
2.2
τ (ns)
FRET efficiency (%)
**
*
Untreated
WT
mutBC
C
TNFR1
TRADD
RIPK1
TRAF2
TNFα
TNFR1
TRADD
RIPK1
TRAF2
NF-κB
TNFα
TNFR1
MEKK1
TRADD
RIPK1
TRADD
RIPK1
MEKK1
TRAF2
NF-κB
p38
JNK

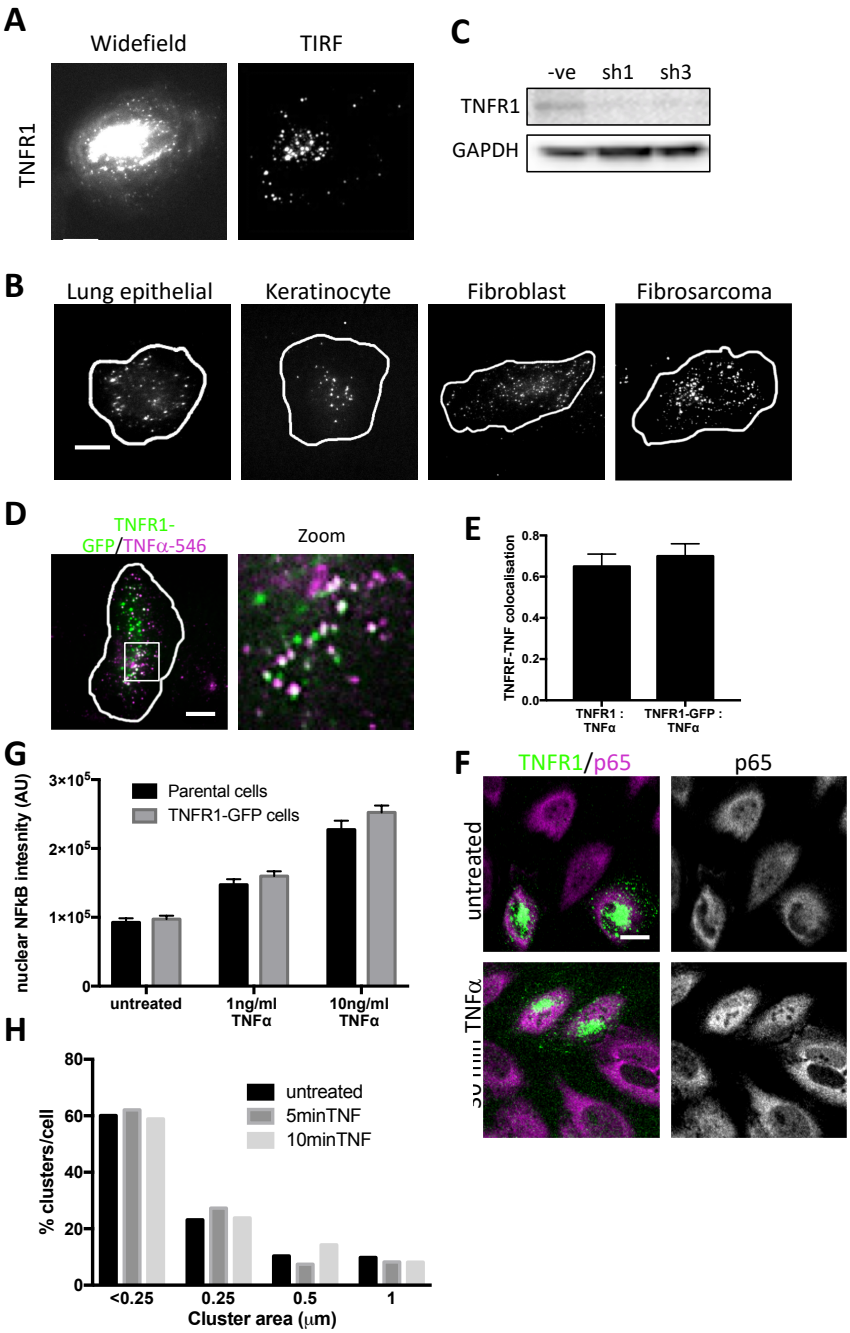

Figure S1: TNFR1 clusters occur in multiple adherent cell types
(A) Widefield and corresponding TIRFM images of HeLa cells expressing TNFR1-GFP. Images are representative of 6 independent experiments. (B) TIRFM images of specified cell types stained with anti-TNFR1 antibodies. White lines around cells denote plasma membrane boundary. Images are representative of 4 independent experiments. (C) Western blot of TNFR1 levels in HeLa cells expressing non-targeting control shRNA (-ve) and two different TNFR shRNA plasmids (sh1, sh3). Blots are representative of 4 independent experiments. Sh3 cells were used in all subsequent experiments to re-express TNFR1-GFP. (D, E) TIRFM images of TNFR1-GFP (green) expressing HeLa cells treated with TNFα-Alexa546 (10ng/ml; magenta). Quantification of colocalization between TNFR1-GFP or endogenous TNFR1 with TNF from 60 cells across 4 independent experiments. Image representative of 4 independent experiments. (F and G) Confocal microscopy images of TNFR1-GFP (green) expressing sh3 HeLa cells treated with TNFα treated (10ng/ml, 30 mins) fixed and stained for phospho-p65 (p65; magenta). Quantified nuclear NFκB in Parental HeLa or sh3HeLa expressing TNFR1-GFP treated with 1ng/ml or 10ng/ml TNFα. Data is from 10 fields of view in one experiment; images (F) and graph are representative of 4 independent experiments. Mean values +/- SEM are shown in graph. (H) Quantification of TNFR1 cluster area and number per cell from parental HeLa fixed and stained for endogenous TNFR1. Data is pooled from 30 cells over 3 independent experiments. Scale bars are 10μm throughout.

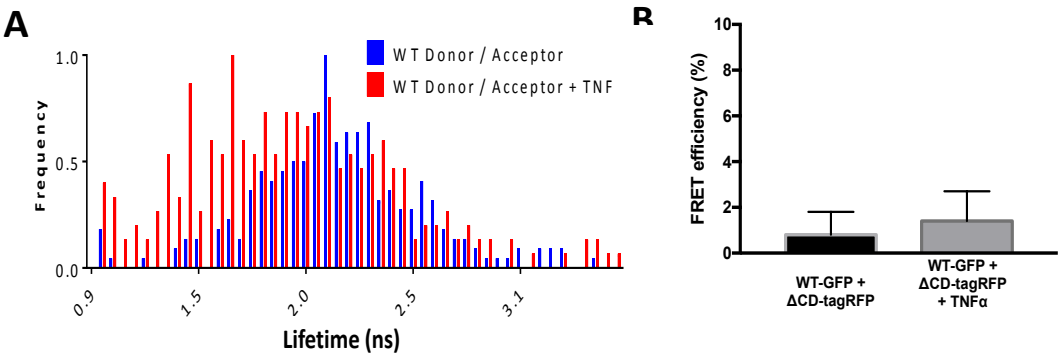

Figure S2: TNFR1 molecules increase homotypic associations in response to ligand binding

(A) Histogram of lifetime distribution relative to frequency of lifetime in HeLa cells co-expressing WT TNFR-GFP and WT TNFR-RFP untreated or treated with 10ng/ml TNFα. Data is from images of 10 cells and representative of 3 independent experiments (10 cells per experiment). (B) Graph of FRET efficiency of HeLa cells co-expressing WT TNFR-GFP and ΔCD TNFR1-RFP without or with 5 min treatment with 10ng/ml TNFα. Graph shows mean FRET efficiency +/- SEM from 10 cells per condition and is representative of 3 independent experiments (10 cells per experiment).

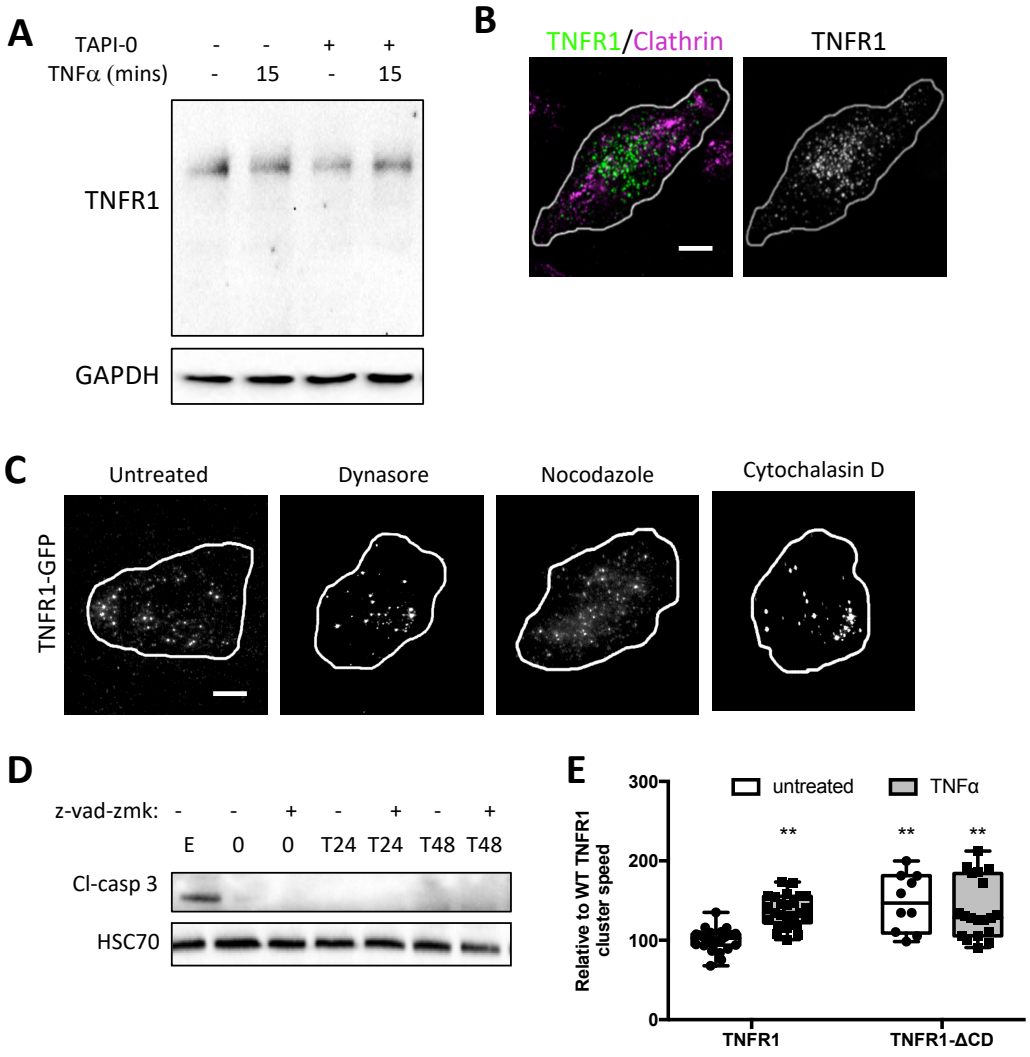

Figure S3: TNFR1 clusters do not require membrane microdomains or cytoskeleton for assembly

(A) Western blot of HeLa cells treated without or with 15 min treatment with 10ng/ml TNFα in the presence or absence of pre-treatment with the TACE inhibitor TAPI-0. Representative of 4 independent experiments. (B) TIRFM image of TNFR1-GFP expressing HeLa cell (green) stained with antibodies to clathrin (magenta). White lines around cells denote plasma membrane boundary. Representative of 3 independent experiments. (C) TIRFM images of WT or ΔCD TNFR1-GFP expressing HeLa cells treated with Dynasore (80μM, 1h), Nocodazole (10μM, 20 mins) or Cytochalasin D (1μm, 15 minutes). Representative of 4 independent experiments. (D) Western blot of HeLa cells with or without 10ng/ml TNFα in the presence or absence of z-vad-zmk caspase inhibitor. Etoposide (E) was used as a positive control. Cells were lysed at time 0 or after 24 or 48 hours and probed for cleaved caspase-3. Representative of 4 independent experiments. (E) Quantified TNFR1-GFP cluster speed from TIRFM movies over 10 minutes with or without 10ng/ml TNFα treatment. Median values are shown on graphs as a line with upper and lower quartiles noted. * denotes $p<0.01$ by 2-way ANOVA. Scale bars are 10μm throughout.

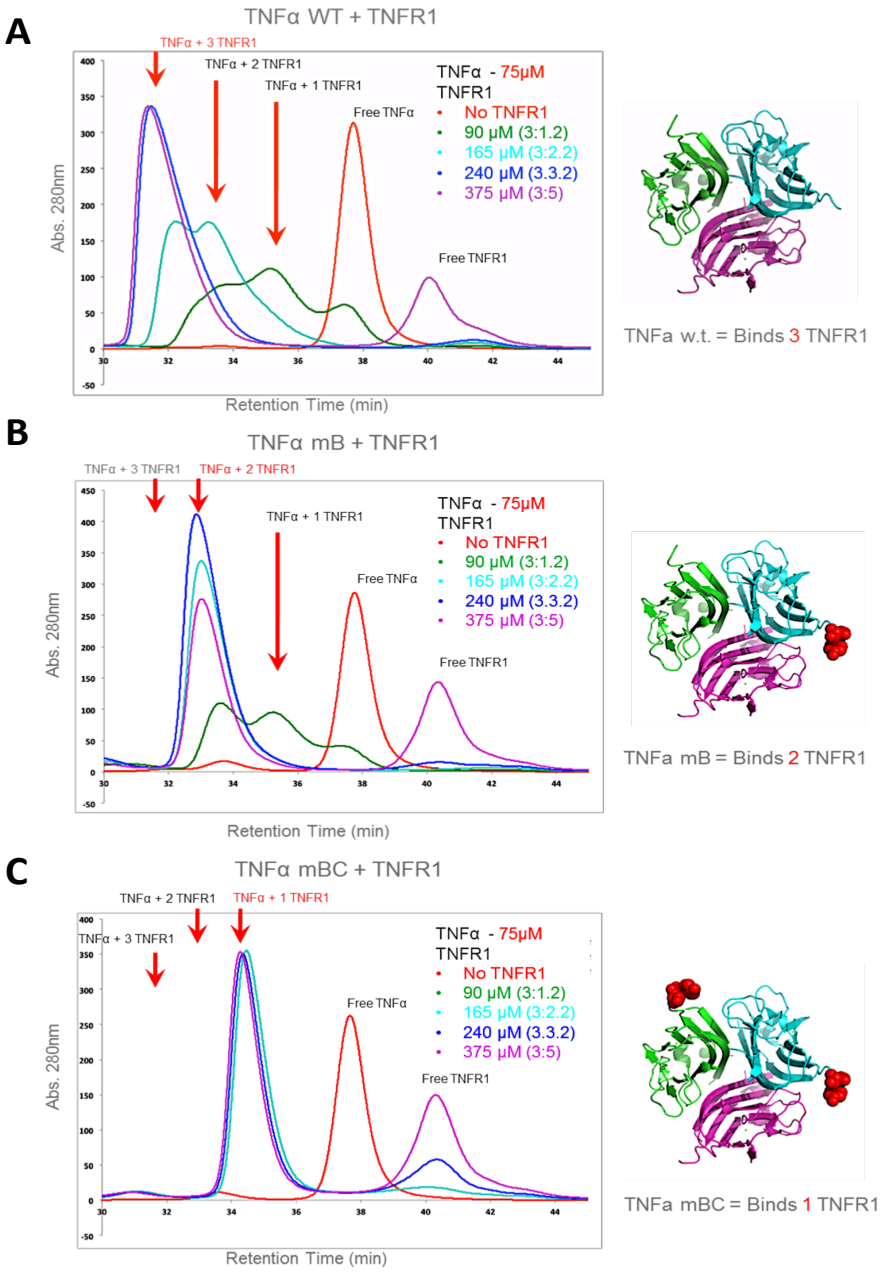

Figure S4: Analytical size exclusion chromatography (AnSEC) analysis of titration of TNFR1 with scTNFα

(A-C): AnSEC analysis traces of wild-type scTNFα (A), mBTNFα (B) or mBCTNFα (C) alone (red traces), and combined with hTNFR1 over a range of ratios (TNF ,trimer: TNFR1): 1:1.2, 1:2.2, 1:3.2 and 3:5 (green, cyan, blue and purple traces respectively). Peaks corresponding to TNFα bound to 1, 2 or 3 receptors indicated by red arrows. In addition to the main peaks of 1 and 2 receptors bound at sub-saturating concentrations of receptor (1.2x and 2.2x; green and cyan traces respectively), shoulders on these peaks indicate the presence of all possible complex stoichiometries as the mix establishes a state of equilibrium. Cartoons adjacent to each AnSEC trace in A-C show the TNFα trimer with the mutated residues shown as red spheres.

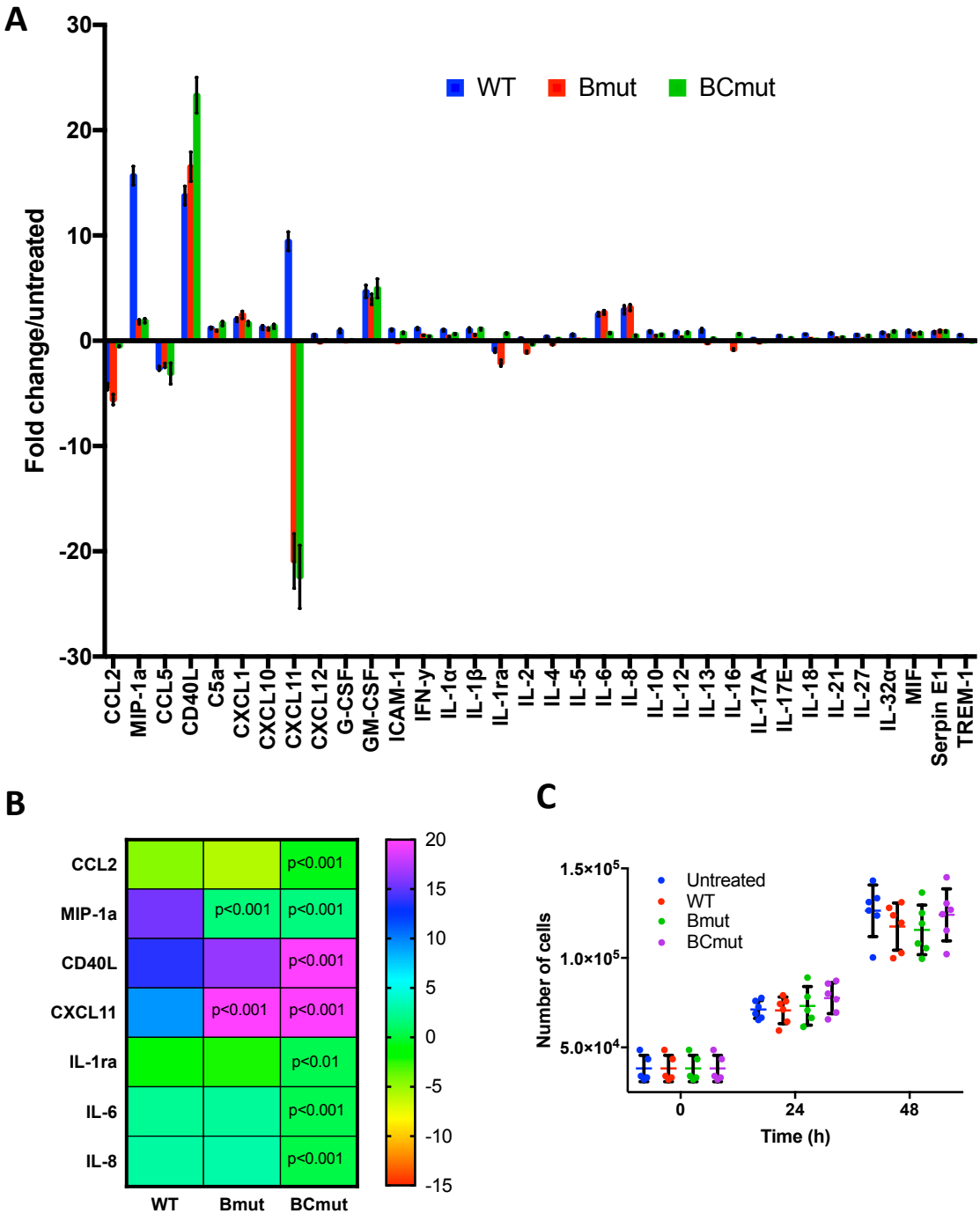

Figure S5: Differential cytokine release in response to mutant scTNFα binding
(A) Profile of cytokine release from cells treated with scTNFα (WT, blue bars) or mutant forms (Bmut, red bars and BCmut, green bars) for 8h. Values are shown as fold change over untreated cells over the same time period, pooled from duplicate arrays per experiment and two independent experiments. Mean values+/-SEM are shown from 2-way ANOVA. (B) Heatmap showing fold change of cytokines noted as significantly different across treatment conditions with associated p values. (C) Analysis of proliferation of HeLa cells untreated or treated with WT or mutant TNF over time. Data is pooled from tile scan cell counts from 6 wells per condition (individual data points are shown with the black bar denoting the mean +/-SEM) and is representative of 5 independent experiments.

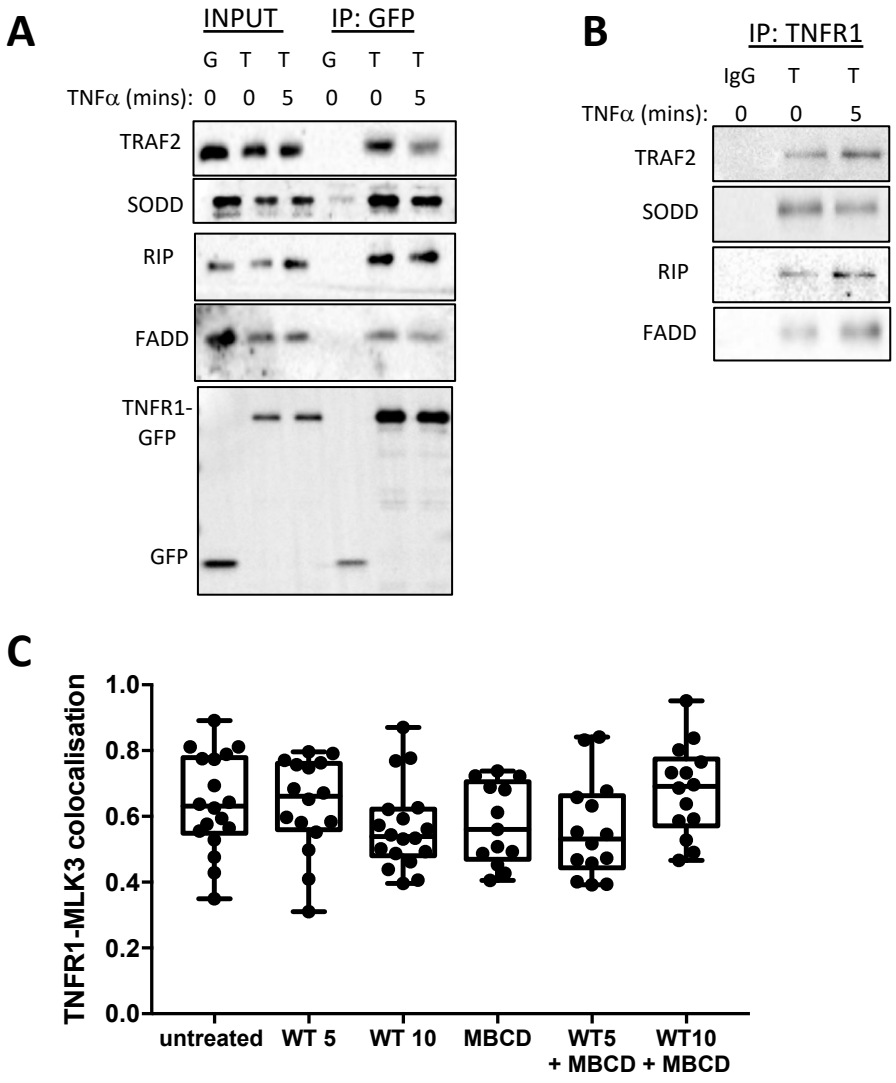

Figure S6: TNFR1 clusters do not change association with complex I proteins or MLK3 in response to TNF

(A) Western blots of whole cell lysates (input) or GFP IP samples (IP) from cells expressing GFP only (G) or WT TNFR1-GFP (T) untreated or treated with TNFα. Data is representative of 4 independent experiments. (B) Western blots of TNFR1 IP samples from HeLa cells starved (0) or treated with TNFα were probed for specified proteins. IgG was used as a control for non-specific binding. Data is representative of 3 independent experiments. (C) Quantification of TNFR1-GFP colocalization co-efficient with endogenous MLK3 stained with alexa-568 secondary antibodies from TIRFM images. Cells were treated with WT TNF for 0, 5 or 10 mins with or without pre-treatment with MβCD as noted. Median values from >13 images per condition are shown on graphs as a line with upper and lower quartiles noted and all data points. Data is representative of 3 independent experiments.